Prepared in cooperation with the Bureau of Reclamation

Electrical Resistivity Investigation of Fluvial Geomorphology to Evaluate Potential Seepage Conduits to Agricultural Lands along the San Joaquin River, Merced County, California, 2012–13

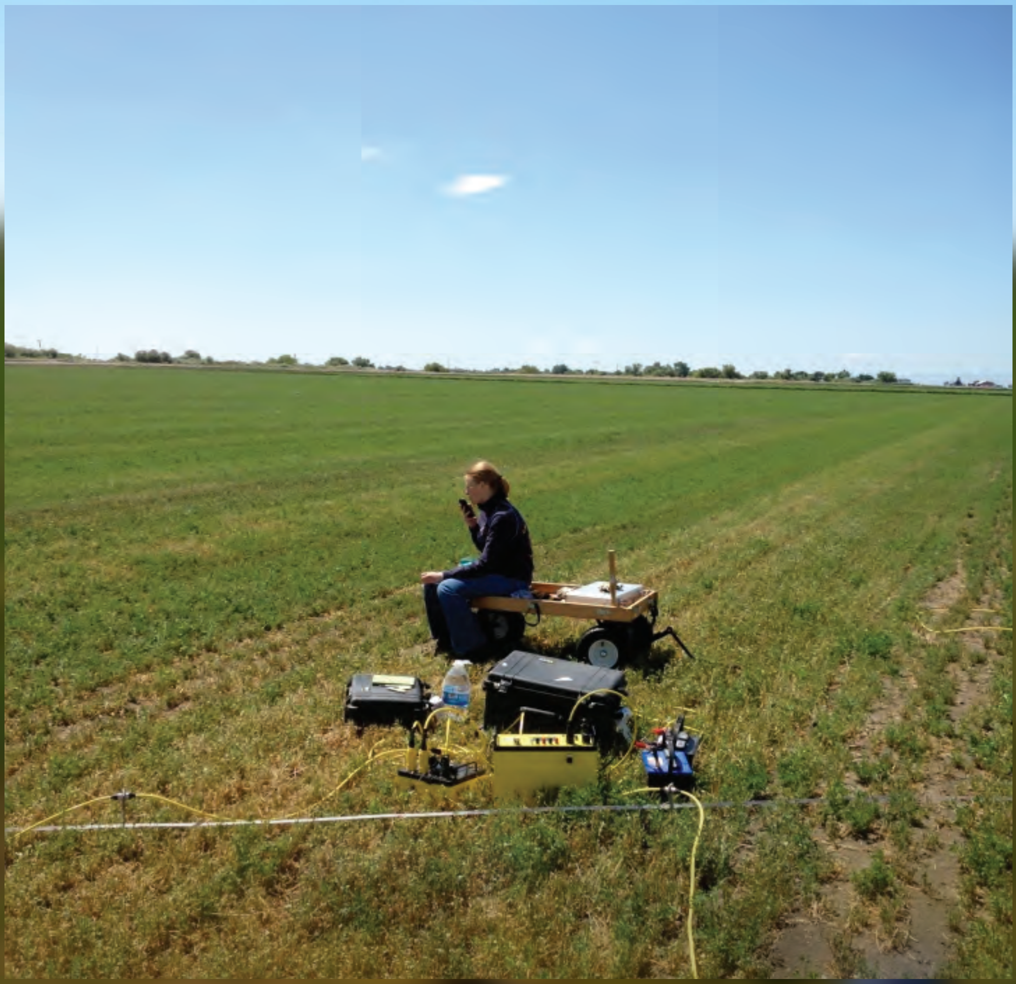

Scientific Investigations Report 2016–5172

U.S. Department of the Interior
U.S. Geological Survey

Cover. Direct-current resistivity measurements being collected in an agricultural field near the San Joaquin River, Merced County, California, 2012.

Electrical Resistivity Investigation of Fluvial Geomorphology to Evaluate Potential Seepage Conduits to Agricultural Lands along the San Joaquin River, Merced County, California, 2012–13

By Krishangi D. Groover, Matthew K. Burgess, James F. Howle, and Steven P. Phillips

Scientific Investigations Report 2016–5172

U.S. Department of the Interior
U.S. Geological Survey

U.S. Department of the Interior
SALLY JEWELL, Secretary

U.S. Geological Survey
Suzette M. Kimball, Director

U.S. Geological Survey, Reston, Virginia: 2016

Suggested citation:
Groover, K.D., Burgess, M.K., Howle, J.F., Philips, S.P., 2017, Electrical resistivity investigation of fluvial geomorphology to evaluate potential seepage conduits to agricultural lands along the San Joaquin River, Merced County, California, 2012–13: U.S. Geological Survey Scientific Investigations Report 2016–5172, 39 p., https://doi.org/10.3133/sir20165172.

ISSN 2328-0328 (online)

Acknowledgements

The authors acknowledge the contributions of Katrina Harrison and Allison Warren, Bureau of Reclamation, for their help in the field and the planning of the surveys.

The authors also acknowledge the contributions of Adam Kjos and Andy Morita, U.S. Geological Survey, for field help. We thank Matthew Landon, Michelle Sneed, Christopher Hobza, and James Callegary for constructive manuscript reviews.

Contents

Figures

Figures—Continued

Tables

Conversion Factors

SI to Inch/Pound

Multiply	By	To obtain
	Length	
centimeter (cm)	0.3937	inch (in.)
millimeter (mm)	0.03937	inch (in.)
meter (m)	3.281	foot (ft)
kilometer (km)	0.6214	mile (mi)
	Pressure	
kilopascal (kPa)	0.009869	atmosphere, standard (atm)
kilopascal (kPa)	0.1450	pound per square inch (lb/ft2)
	Energy	
milliamps (mA)	0.001	watt/volt
millivolt (mV)	0.001	volts
ohm-meters (ohm-m)	0.001	kiloohm-meters (kohm-m)

Electrical conductivity σ in siemens per meter (S/m) can be converted to electrical resistivity ρ in ohm-meters (ohm-m) as follows: $\rho = 1/\sigma$.

Electrical resistivity ρ in ohm-meters (ohm-m) can be converted to electrical conductivity σ in siemens per meter (S/m) as follows: $\sigma = 1/\rho$.

Vertical coordinate information is referenced to the North American Vertical Datum of 1988 (NAVD 88).

Horizontal coordinate information is referenced to the North American Datum of 1983 (NAD 83).

Elevation, as used in this report, refers to distance above the vertical datum.

Abbreviations

DC	direct current
EC	electrical conductivity
HPT	hydraulic profiling tool
kohm-m	kiloohm-meters
ohm-m	ohm-meters
RMSE	root mean squared error
USGS	U.S. Geological Survey
2D	two-dimensional
3D	three-dimensional

Electrical Resistivity Investigation of Fluvial Geomorphology to Evaluate Potential Seepage Conduits to Agricultural Lands along the San Joaquin River, Merced County, California, 2012–13

By Krishangi D. Groover, Matthew K. Burgess, James F. Howle, and Steven P. Phillips

Abstract

Increased flows in the San Joaquin River, part of the San Joaquin River Restoration Program, are designed to help restore fish populations. However, increased seepage losses could result from these higher restoration flows, which could exacerbate existing drainage problems in neighboring agricultural lands and potentially damage crops. Channel deposits of abandoned river meanders that are hydraulically connected to the river could act as seepage conduits, allowing rapid and widespread water-table rise during restoration flows. There is a need to identify the geometry and properties of these channel deposits to assess their role in potential increased seepage effects and to evaluate management alternatives for reducing seepage. Electrical and electromagnetic surface geophysical methods have provided a reliable proxy for lithology in studies of fluvial and hyporheic systems where a sufficient electrical contrast exists between deposits of differing grain size. In this study, direct-current (DC) resistivity was used to measure subsurface resistivity to identify channel deposits and to map their subsurface geometry. The efficacy of this method was assessed by using DC resistivity surveys collected along a short reach of the San Joaquin River in Merced County, California, during the summers of 2012 and 2013, in conjunction with borings and associated measurements from a hydraulic profiling tool.

Modeled DC resistivity data corresponded with data from analyses of core samples, hand-auger samples, a hydraulic profiling tool, and aerial photographs, confirming that DC resistivity was effective for differentiating between silty and sandy deposits in this setting. Modeled DC resistivity data provided detailed two-dimensional cross-sectional resistivity profiles to a depth of about 20 meters. The distribution of high-resistivity units in these profiles was used as a proxy for identifying areas of high hydraulic conductivity. Estimates of the cross-sectional area of channel deposits from DC resistivity pseudosections can provide critical input for groundwater-flow models designed to simulate river seepage and evaluate seepage-management alternatives.

Introduction

Increased flows in the San Joaquin River, part of the San Joaquin River Restoration Program, are designed to restore salmon and other fish populations while reducing or avoiding adverse water-supply effects from these higher than previous restoration flows (San Joaquin River Restoration Program webpage, http://restoresjr.net/index.html, accessed on July 23, 2014). Seepage losses resulting from the increased flows could exacerbate existing drainage problems in neighboring agricultural lands, however, which could damage crops from waterlogging, increased salinity in the root zone, or both. Channel deposits of abandoned river meanders that are hydraulically connected to the river can act as seepage conduits, allowing for rapid and widespread water-table rise during restoration flows. Identifying and characterizing the channel deposits to assess potential seepage will help to evaluate management alternatives for reducing seepage.

Electrical and electromagnetic surface geophysical methods have provided a reliable proxy for lithology in studies of fluvial and hyporheic systems where a sufficient electrical contrast exists between deposits of differing grain size (Froese and others, 2005; Bowling and others, 2006; Bersezio and others, 2007; Callegary and others, 2007; Nyquist and others, 2008; Minsley and others, 2010; Brosten and others, 2011; Cardenas and Markowski, 2011). The Bureau of Reclamation (Reclamation) partnered with the U.S. Geological Survey (USGS) to apply electrical and electromagnetic geophysical methods at sites along Reach 4A of the San Joaquin River, approximately 25 kilometers (km) east of the city of Los Banos, California, between Sack Dam and the Sand Slough Control Structure (fig. 1; McBain and Trush, Inc., 2002), to investigate the fluvial geomorphology of the agricultural land that is subject to seepage from restoration flows.

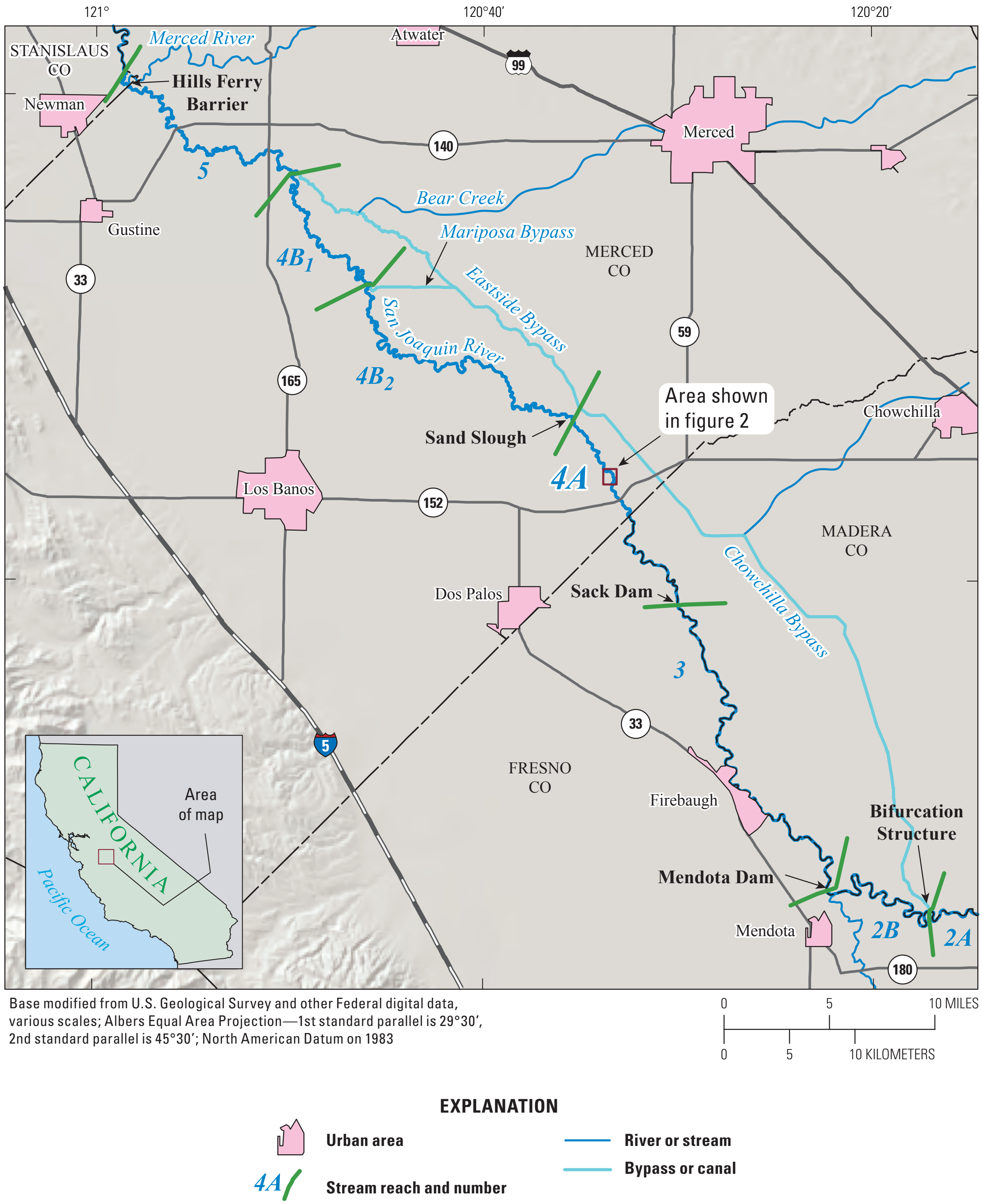

Figure 1. Location of Reach 4A along the San Joaquin River in Merced, Fresno, and Madera Counties, California.

The purpose of this report is to present interpreted direct-current (DC) resistivity data from surveys that were done in agricultural fields near the active channel of the San Joaquin River (fig. 2). The study area consisted of three agricultural fields (referred to as fields 1 through 3) adjacent to the San Joaquin River with abandoned river meanders identifiable in aerial photographs. These abandoned river meanders were investigated to evaluate the textural and morphological differences between the channels and surrounding overbank deposits, and assess the hydrologic connection between the abandoned meanders and the active channel of the San Joaquin River. Interpretation of the geophysical data was constrained by other types of co-collected data. These data included analyses of cores, hand-auger samples, direct-push hydraulic profiling tool (HPT) logs, and aerial photographs. Modeled DC resistivity data provided detailed two-dimensional cross-sectional resistivity profiles to a depth of about 20 meters (m). The distribution of high-resistivity units in these profiles was used as a proxy for identifying areas of high hydraulic conductivity. These data were subsequently used to guide the location and depth of wells installed for monitoring groundwater flow in the channel deposits.

Study Area

The area along Reach 4A of the San Joaquin River (figs. 1, 2) is actively used agricultural land. Inspection of aerial photographs revealed multiple sinuous lines of reduced crop productivity that corresponded to abandoned river meanders (fig. 2). The reduced crop productivity in the abandoned meanders could result from one or a combination of factors, including differences in soil properties, such as relatively low organic-matter content, rapid drainage or poor retention of irrigation water where the unsaturated zone is composed of clean (well-sorted) sands, and the presence of shallow groundwater during high river flows. Geologic investigations in fields 1 and 2 (fig. 2) confirmed that a textural contrast exists between the surficial trace of the channel deposits (well-sorted medium sands) and the banks of the abandoned channels (silty loam; A. M. Warren, Bureau of Reclamation, written commun., January 25, 2013; A. Kjos, U.S. Geological Survey, written commun., September 18, 2013).

Three agricultural fields that had identifiable abandoned channels in aerial photographs (fig. 2) compose the study area. All areas of the fields (including the abandoned meanders) were overlain by 0.3 m of relatively fine-grained tilled soil. Cultivation of these lands could have facilitated some redistribution of surficial deposits, resulting in the fine-grained cap of tilled soil.

Fluvial Geomorphology

The fluvial geomorphology of the San Joaquin River system in Reach 4A is characterized by the active channel incising through its floodplain sediment sequences of overbank flood-plain deposits and abandoned meanders. Abandoned meanders are typically filled with cross-bedded point bars deposited through lateral accretion, and coarse-grained channel deposits. Point bars form on the inside bends of a vigorously meandering channel, where the stream velocity is slower (Easterbrook, 1993). Meander abandonment is associated with the development of cutoffs. During flooding events, flow across the point bar can establish chute channels. Scouring of these chutes can lead to the establishment of a new channel across the point bar and abandonment of the meander (Mount, 1995). Chute channels were observed on multiple point bars in the active channel next to the study area. During major floods, an undammed river will occasionally abandon its active channel entirely and establish a new channel in the surrounding floodplain (Mount, 1995). Such large-scale channel abandonment, known as avulsion, is a common process in most large and intermediate unmanaged river systems, including the San Joaquin River prior to the 20th century (Mount, 1995). Flooding events can also result in crevasse splay deposits, which are composed of relatively coarse-grained, poorly sorted sediment, and are deposited near where the river broke through its levees and changed course (Boggs, 2006).

Electrical Properties of Earth Materials

Electrical resistivity, expressed in units of ohm-meters (ohm-m), is the resistance to an electrical current flowing through an object as a result of an applied potential (voltage) difference, independent of the object geometry, and is an intrinsic material property. The main factors that affect the resistivity of earth materials are (1) the amount of interconnected pore water, (2) the salinity of the pore water, (3) the amount of clay, and (4) the fraction of metallic minerals. The combination of these factors results in a range of resistivity values for typical earth materials that spans many orders of magnitude. Although this large range in resistivity values can be useful for delineating different lithologic units, there is a great amount of overlap among different materials, as well as variability for a single material, which can lead to ambiguity when interpreting resistivity values in a geologic context (Minsley and others, 2010). Extensive discussions about the theory and applications of the electrical properties of earth materials are widely available in the literature (Archie, 1942; Telford and others, 1990; Reynolds, 1997; Binley and Kenma, 2005; Minsley and others, 2010).

Figure 2. Study area west of the active San Joaquin River, Merced County, California, with field numbers and showing locations of direct-current resistivity lines and hydraulic profiling tool surveys. Sinuous traces of abandoned meanders are visible throughout the image, including areas not discussed in this report. Abandoned channel meanders are highlighted with dashed white lines.

Most rock-forming minerals have high resistance to the flow of electrical current. In unconsolidated sediments, high electrical resistivity is associated with coarse-grained deposits, where the bulk of the volume is dominated by insulating minerals. Conversely, low resistivity corresponds to smaller grain sizes, because the larger surface area per unit volume of fine-grained particles promotes transmission of electrical current (Biella and others, 1983; Kwader, 1985). The resistivity of unconsolidated sediment can be lowered by increasing the amount of pore water. When clays are present in unconsolidated sediments, even in small percentages, the resistivity is reduced because of surface conduction effects associated with the atomic structure of clay minerals (Moore and Reynolds, 1997).

The fluvial deposits examined for this study varied substantially in grain size and associated resistivity. The HPT borings encountered deposits on opposite ends of the resistivity scale: high-resistivity (greater than 200 ohm-m) channel deposits composed of medium-to-coarse sand, and low-resistivity (less than 50 ohm-m) silty-clay floodplain deposits. Because the water table was well below the contact between the channel deposits and underlying flood-plain deposits when resistivity and HPT data were collected (K. Harrison, Bureau of Reclamation, written commun., May 14, 2013), the variations in resistivity observed in the data interpreted in this report were primarily a function of the contrasts in grain size and not of large variations in pore water saturation or the detection of the top of the water table.

The relation between particle-size distribution in soils and hydraulic conductivity is well established (Zeleke and Si, 2005); under well-understood conditions, particle-size and electrical resistivity distributions have been used together to estimate the spatial distribution of hydraulic conductivity (Wojnar and others, 2013). The density of lithologic data collected for this study did not allow for a direct correlation between electrical resistivity and hydraulic conductivity; however, assuming that the bottom elevation of the channel deposits is in the unsaturated zone, a reasonable correlation of resistivity to particle size can then be interpolated between lithologic data collection points. A first-order approximation of hydraulic conductivity from the resistivity models can then be made for general engineering purposes or field-scale groundwater-flow modeling.

Methods

The fundamentals of each method of subsurface investigation done in the study area are discussed in the following sections.

Hydraulic Profiling Tool

In September 2013, a direct-push drilling rig with an HPT, manufactured by Geoprobe®, was used in the study area to construct vertical HPT profiles to help characterize the abandoned channel in the subsurface. The HPT data were collected along a transect perpendicular to the axis of the abandoned channel near the southern end of field 1 (fig. 2). This study used the HPT data in a similar manner to the procedure outlined in McCall and others (2009).

The HPT injects water into the formation to measure the pressure response, which can be inversely correlated to hydraulic permeability. The tool also measures fluid electrical conductivity (EC, the reciprocal of resistivity), which, together with hydraulic permeability, can be used as a proxy for lithology. The HPT was used to collect a continuous vertical profile to depths of 13 m in this study. The HPT data were then applied to DC resistivity profiles from the immediate area to constrain the relationship between grain size and electrical characteristics at the study location. The HPT profiles along line 2 examined one of the deepest parts of the channel (HPT1; fig. 2) and a shallower section on the western edge of the channel (HPT2; fig. 2).

A 7.6 centimeter (cm) diameter continuous core was collected at HPT1 using the direct-push drilling rig to a depth of 6 meters. The core location was sited at the 42-m data collection site on line 2. Results from HPT1 and HPT2 are presented in the “Observations and Data” section of this report.

Direct-Current Resistivity

The DC resistivity surveys were collected by using a SuperSting R8 resistivity/induced polarization meter (Advanced Geosciences, Inc., 2011). The DC resistivity measurements were done by injecting a known current into the subsurface through two “transmitter” current electrodes and then measuring the resulting voltage difference between two “receiver” electrodes (fig. 3). Each solid stainless-steel electrode is about 45 cm long and 1 cm in diameter. Each electrode can work either as a transmitter or receiver electrode as the combination of electrode pairs used to make measurements is translated along the line. In this two-dimensional (2D) survey, an initial array of 56 electrodes was laid out in a straight line at regular intervals of 2 m (fig. 3). Information about lateral variability in the subsurface is gained as different combinations of electrode transmitter/receiver pairs are translated across the array while the instrument reads from a command file. In this same manner, information about greater depths can be obtained by increasing the distance between transmitter and receiver electrodes (fig. 3; Minsley and others, 2010).

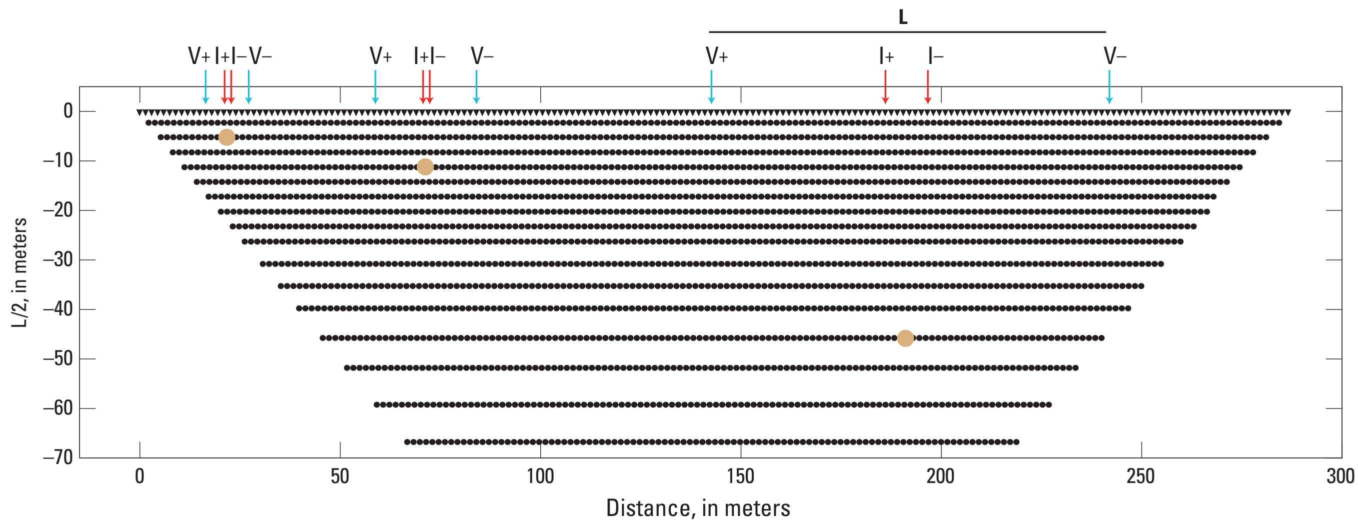

Figure 3. Diagram showing two-dimensional direct-current resistivity acquisition: each point represents a four-electrode measurement and is plotted at the center of the four electrodes at a "depth" equal to one-half of the outer electrode spacing (L/2). The colored points illustrate the effective depth of measurement for each electrode configuration shown at the top of the profile.

An "Inverse Schlumberger" array geometry was utilized for this survey. In this geometry, four electrodes were placed symmetrically around a central location, as depicted in figure 4. For each central transmitter pair, up to 22 variably spaced receiver pairs were used to gain depth information. An apparent resistivity value was calculated for each point from the injected current, measured voltage, and electrode geometry by using equations developed with the assumption of a homogeneous and isotropic earth (Keller and Frischknecht, 1966). Apparent resistivities were plotted at the center of each four-electrode array and at a "depth" equal to one-half of the outer electrode spacing (L/2; fig. 3). Note, however, the voltage used to calculate apparent resistivity is actually a complexly weighted function of the resistivity variations within a volume of soil or rock that influence and, in turn, are sampled by the injected current (Furman and others, 2003).

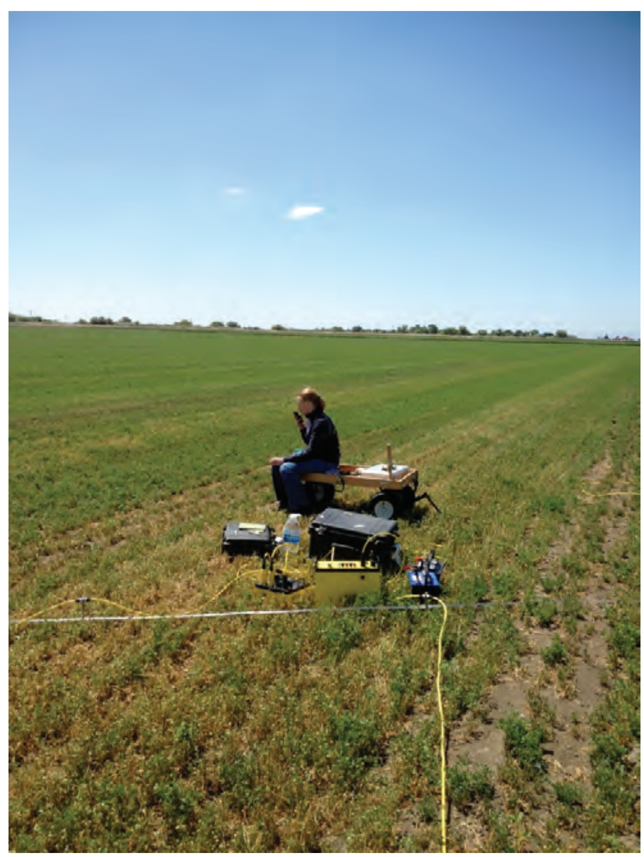

Figure 4. Photograph showing direct-current resistivity meter set up with 2-meter electrode spacing on line 2 near the San Joaquin River, Merced County, California, 2012.

The resistance of the coupling between the electrode and the earth, known as contact resistance, was measured prior to data collection at each location. The measured contact resistance varied depending on the location of the resistivity profile. It typically ranged between a few hundred ohm-meters to more than 8 kiloohm-meters (kohm-m) occasionally, but most contact resistances were less than 1 kohm-m. When resistances greater than 2 kohm-m were measured, the bases of the electrodes were soaked with a saline solution to further decrease the contact resistance (typically less than 500 ohms after application of the solution). A contact resistance of less than 1 kohm-m is optimal (Advanced Geosciences Inc., 2011); based on a large body of field work, the USGS Office of Groundwater, Branch of Geophysics, established contact resistances of less than 1 kohm-m as 'very good,' contact resistances less than 5 kohm-m as 'good,' and contact resistances of between 5 and 10 kohm-m as 'fair' (U.S. Geological Survey Office of Groundwater, Branch of Geophysics, written commun., 2008).

Electrode positions for the majority of the resistivity profiles were measured by using a high-precision Global Positioning System, or GPS (Trimble R7 and R8), which determines horizontal position to within 1.8 cm. The Trimble GPS was not available during collection of line 4; the location data for line 4 were measured by using a handheld GPS with a greater uncertainty in horizontal accuracy (less than 15 m).

The DC resistivity surveys were numbered according to the order in which they were collected (table 1). Surveys 1 through 4 were designed to cross the abandoned channels in fields 1 and 2 (fig. 2) perpendicular to the channel axis identified in aerial photographs to determine the contrast in electrical properties between the channel deposits and the surrounding floodplain. Survey 5 was collected in the dry, active San Joaquin River channel just east of the study area to investigate the resistivity structure beneath the river. Survey 6 was collected parallel to the channel axis of a chute channel on a sandy point bar west of the active channel. Surveys 7 through 9 were collected from each field, across the unlined irrigation canal and into point-bar deposits (either currently or formerly active) on the west bank of the active channel; electrodes were held in position at the surface of the water in the canal by using rope and foam floats (fig. 5). Surveys 10 through 12 crossed the abandoned channel in fields 1 and 3, parallel to the crop rows. These last three lines were collected, in part, to serve as a calibration for frequency-domain electromagnetic (FDEM) data (Minsley and others, 2012) that were also collected throughout the study area (not discussed in this report).

Data were collected with an electrode spacing of 2 m, except for line 6, which was collected by using a 1-m electrode spacing because of space constraints. For certain surveys, the line length was increased from 110 m (56 electrodes at 2-m spacing) by moving one of the eight strands of electrode cables from the beginning of the line to the end after the original data had been collected (by performing a "roll-along") and appending the new data to the original set. This process was repeated as needed to increase the survey to the desired length. The field acquisition parameters are presented in table 1.

Table 1. Summary of data acquisition parameters for direct-current resistivity surveys collected at study area along Reach 4A of the San Joaquin River, Merced County, California, 2012–13.

[m, meters; mm/dd/yyyy; month/day/year]

Line number	Line length (m)	Number of electrodes	Electrode spacing (m)	Location	Collection date (mm/dd/yyyy)
1	110	56	2	Field 2	06/05/2012
2	110	56	2	Field 1	06/06/2012
3	110	56	2	Field 1	06/07/2012
4	182	91	2	Field 1	09/09/2012
5	110	56	2	Active channel	05/07/2013
6	55	56	1	Active channel margin	05/08/2013
7	110	56	2	Field 1	06/11/2013
8	110	56	2	Field 2	06/12/2013
9	110	56	2	Field 3	06/13/2013
10	166	84	2	Field 1	08/27/2013
11	110	56	2	Field 3	08/28/2013
12	124	62	2	Field 1	08/29/2013

Figure 5. Photograph showing direct-current resistivity cables crossing an irrigation canal, Merced County, California. Electrodes were floated on the water surface with foam floats. Electrode spacing remained consistent by marking the distance along the rope pulled tight across the canal.

The raw data (measured apparent resistivity) and forward model (calculated apparent resistivity) pseudosections are shown in appendix 1. Inversion modeling results are shown as 2D sections (resistivity profiles) in the "Direct-Current Resistivity Profiles" section of the report as well as in the appendix figures.

The raw data in the DC resistivity method are voltages converted to apparent resistivity and plotted in pseudosections, and data locations are almost entirely dependent on the electrode geometry. Thus, the arrangement of apparent resistivities plotted in a pseudosection does not accurately reflect the resistivity distribution of the underlying earth. These resistivity pseudosections must be inverted in order to more closely reflect the spatial distribution of resistivity values in the subsurface (Minsley and others, 2010).

Forward modeling and inversion are mathematical techniques used to develop a subsurface resistivity model from the recorded data. Forward modeling refers to the process of predicting resistivity values at various locations for a given resistivity model based on the physics of electrical current flow in resistive media. The forward modeling process is well-posed; that is, there is a unique set of predicted values for a given resistivity model. Inversion refers to the derivation of a resistivity model from the measured data. Resistivity inversion is non-unique; there can be many models that fit the measured data equally. Assumptions were made to constrain the resultant set of models by applying settings in the software interface to prefer solutions favoring sharp variations in resistivity values between neighboring materials to reflect the geologic data. A summary of system parameters used in the data collection and modeling process is provided in table 2.

The data were inverted by using AGI's EarthImager 2D software (version 2.4.0, build 617; Advanced Geosciences Inc., 2009) that both uses damped least squares and smooth inversion modeling routines. A damped least squares inversion method was selected to display the models in this report. This routine was better suited for this study setting, where there was a juxtaposition of units with a contrast in resistivity of over 150 ohm-m, than the smooth model inversion algorithm, which is generally considered more robust. The inversions were allowed to run for a maximum of eight iterations, with stopping criteria of 5 percent or less root-mean-square error (RMSE) between the measured and forward modeled data, or an L2-norm (sum of squares) value of one or less for the error-weighted data misfit. Multiple inversions were run using various data error tolerances and smoothing parameters to assess the stability of the model and to establish inversion parameters that could be applied to all data sets.

Table 2. System parameters used for direct-current resistivity data collection and modeling, 2012–13, Merced County, California.

[cm, centimeters; m, meters; mA, milliamps; mV, millivolts; ohm-m, ohm-meters]

Survey parameters	
Minimum injected current	50 mA
Maximum injected current	800 mA
Measurement time	1.2 seconds
Number of current cycles	2
Array type	Inverse Schlumberger
Electrode spacing[1]	1 m, 2 m
Total electrode length	45 cm
Electrode diameter	1 cm
Electrode depth for 1 meter spaced line	10 cm
Electrode depth for 2 meter spaced line	20 cm
Minimum. number of electrodes utilized	56
Maximum number of electrodes utilized	112
Data removal criteria	
Minimum voltage	0.2 mV
Maximum repeat error	3 percent
Minimum apparent resistivity	1 ohm-m
Maximum apparent resistivity	10,000 ohm-m
Resistivity inversion	
Inversion method	Damped least squares
Maximum number of iterations	8
Maximum root mean squared error	5 percent
Smoothness factor	10
Damping factor	10
Horizontal/vertical roughness ratio	0.5

[1]Electrode spacing varied among surveys; see table 1 for details.

Observations and Data

For organizational purposes, this section discusses the results of each of the methods of subsurface investigation separately.

Hydraulic Profiling Tool Profiles

Inspection of the vertical profile generated at HPT1 revealed a zone of high hydraulic permeability (low tool pressure) from land surface to a depth of 4 m (fig. 6). An abrupt decrease in hydraulic permeability below 4-m-depth corresponded to the contact between the overlying channel and the underlying floodplain deposits. This sharp contact was clearly observed in the continuous core, also at a depth of 4 m, and is shown by the dashed line in figure 7. The top 0.3 m of the core consisted of tilled topsoil. Medium to coarse-grained sand, with minor 6–10 cm-thick, fine-textured bedding planes, was encountered from 0.3 to 4 m below land surface. Minor laminations of silty sand and sandy gravel were present throughout the sandy interval. The bottom of the sand was characterized by an abrupt contact with silty clay at 4 m; the clay was present for the rest of the cored interval (to about 6 m below land surface). The continuous core only extended to a total depth of 6 m, but comparison of the lithology log generated from the core and the vertical profile collected at HPT1 indicated that the fine-grained deposits were present to the bottom of the hole at 13 m. Variability in the HPT1 data within the fine-grained deposits indicated the possibility of interbedded coarser-grained horizons, possible variations in salinity below the water table at a depth of about 9.2 m, or both.

HPT2 (fig. 8) was less than 10 m to the northwest of 24 m on line 2, near the western bank of the abandoned channel (fig. 2). In this location, the channel deposits were interbedded with floodplain deposits: coarse channel deposits were observed to a depth of 2 m and were underlain by 1 m of silty clay. A thinner horizon of probable fine-to-medium sand from 3 m to 3.7 m in depth could represent older channel deposits. Sediment below this depth to 13 m appeared to be fine-grained (silty clay), although small interbeds of coarser materials are possible.

Direct-Current Resistivity Profiles

The final inverted resistivity cross sections were annotated with geologic interpretations based on field observations made during this study. Pseudosections that present the measured data, as well as data predicted by the final inverse model, are provided in the appendix. Channel deposit width was measured from georeferenced aerial photos to constrain interpretation of the resistivity sections. As presented, the vertical scale of the modeled resistivity sections is exaggerated and not equal to the horizontal scale. The vertical scale is the same for all sections, except line 6, which was collected by using a 1-m-electrode spacing. Furthermore, the horizontal scale is not the same for all sections. The EarthImager 2D software did not provide a way to normalize the displayed horizontal scale between surveys of different lengths. Most lines were collected along 110-m transects; however, line 6 was 55-m long, and lines 4, 10, and 12 were longer than 110 m (table 1). The resistivity scale was kept the same for all modeled resistivity sections in figures shown in this section of the report.

The lowest elevation of the 220 ohm-m resistivity contour was selected to approximate the depth of channel deposits on the basis of the HPT data and lithology from the continuous core. A bold, black line was drawn across each modeled resistivity section to illustrate the interpreted bottom of the sand deposits and to clarify that the modeled resistivity below this depth is not expected to be representative of the subsurface because of a shadow effect (Kuznetzov, 1982; Zonge and Hughes, 1988) which masks the true resistivity of the subsurface because of ground-wave distortion relative to a uniform half-space (Yan and Fu, 2004). Areas of moderate resistivity (50–200 ohm-m) beneath this bold line are regions of data uncertainty. On the basis of EC measurements from HPT data (figs. 6, 8), we expected fine-grained deposits beneath the contact to have true resistivity values of less than 50 ohm-m.

The following sections present the inverted resistivity models. Line numbers refer to the order in which the data were acquired. Lines are grouped for presentation on the basis of the field they are in; each field contained at least one abandoned meander visible in aerial photographs (fig. 2). Line 2 is presented first because HPT data were co-located with sites along that line. Subsequent lines collected in fields 1 and 3 are presented from upstream to downstream. Lines that cross from each field over the irrigation canal and into the active channel are presented last in the subsection of the field from which they began. The inverted resistivity profiles showed a strong contrast between high resistivity in the channel deposits and the low resistivity of the surrounding areas.

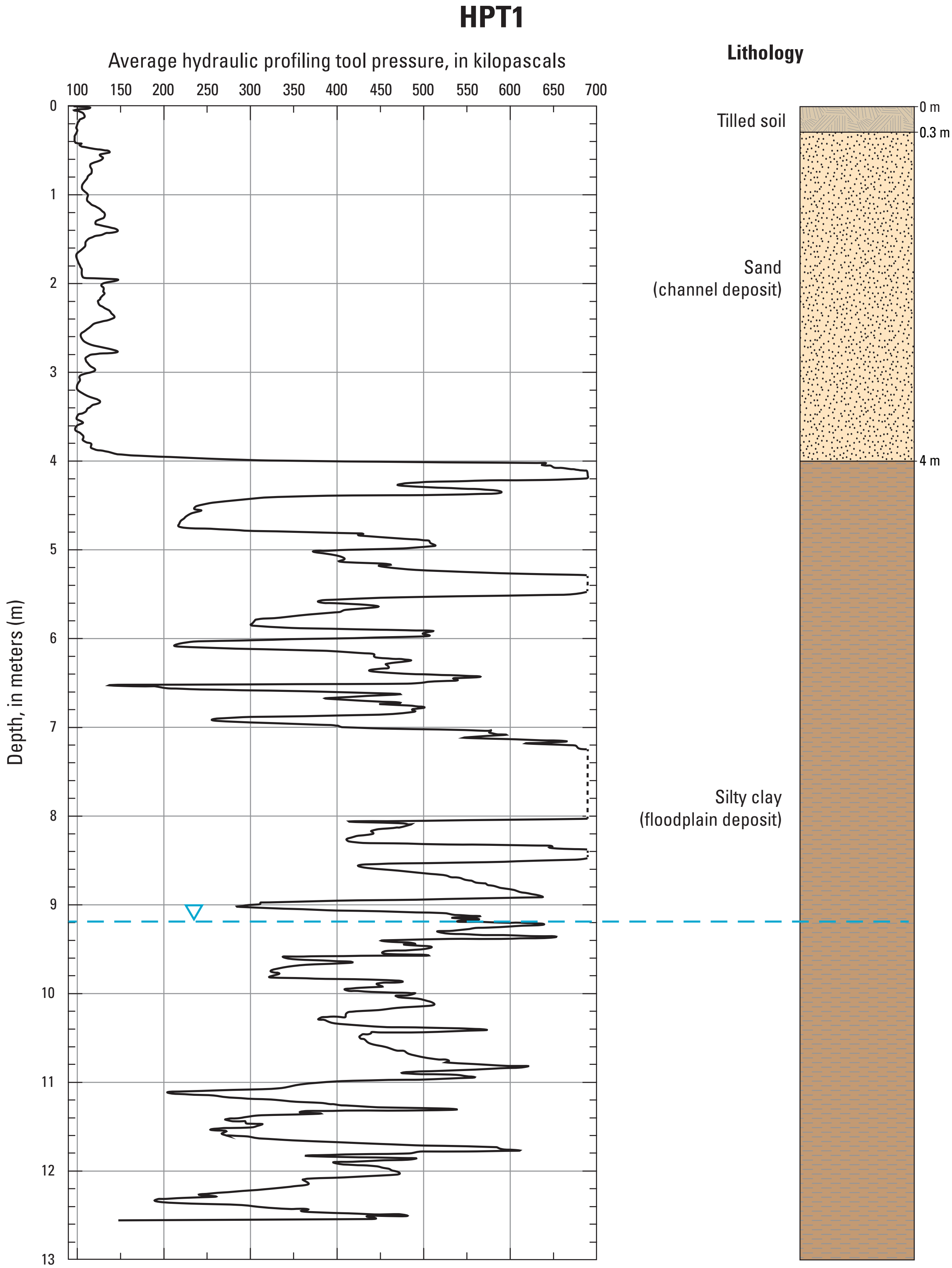

Figure 6. Vertical profile HPT1 generated by hydraulic profiling tool in field 1 (fig. 2) and interpreted lithology, abandoned channel next to the San Joaquin River, Merced County, California, 2013. Dashed line in the hydraulic profiling tool profile indicates where measurement exceeded instrument threshold. Data correlates with 42 meters (m) on line 2.

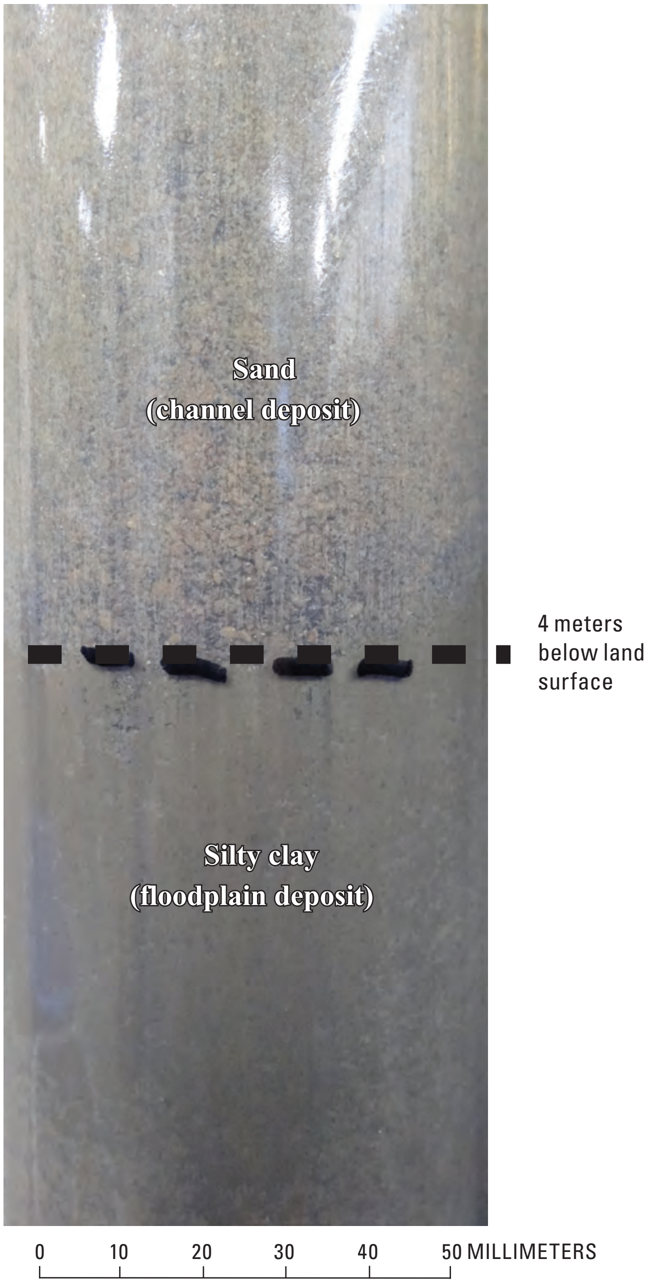

Figure 7. Contact between coarse-grained channel sand and underlying floodplain deposits, in a core collected next to HPT1 (fig. 6), San Joaquin River, Merced County, California.

Field 1

Field 1 consisted of a relatively large northwest-southeast trending cultivated plot of land. An irrigation canal and the San Joaquin River intersect Field 1 at the southeast and northern edges of the field. At least two abandoned channels (visible in aerial photographs) cross the length of this field (fig. 2). Several direct-current resistivity surveys, HPT1, and HPT2 were located within this field.

Line 2

Line 2 data were collected approximately perpendicular to the channel axis, as identified in aerial photographs, at the southeastern edge of field 1 (fig. 2). Figure 9 shows the modeled resistivity data collected with 2-m-electrode spacing along line 2. The channel deposits identified in aerial photographs were visible between 20 and 54 m along line 2 and are nearly 34-m wide. The bottom of the 220 ohm-m contour (yellow) approximated the depth of sand (4 m) encountered at HPT1 at the 42 m electrode site (fig. 6). The contour line used to approximate the area of these sand deposits was drawn by projecting the lowest elevation of the 220 ohm-m contour to the trace of the channel deposits visible at land surface in aerial photographs. The abandoned channel is slightly asymmetric; the deepest deposits are near the inside of the meander on the eastern side of the channel. A shadow effect persisted below the high-resistivity zone centered between 20 and 54 m, caused by the contact between sandy channel deposits and silty floodplain (at a maximum depth of 6 m), extending down to the water table estimated by the HPT (at about 9 m depth).

Sediments of moderate-to-high resistivity present in the upper 4 m of the northeastern end of the profile, centered beneath 96 m along line 2, correlated with coarse-grained deposits visible on the surface in aerial photographs (fig. 2). However, this model showed that the sand deposits in this location are not as resistive or deep as those between 20 and 54 m. These moderately resistive deposits could be crevasse splays that are hydraulically connected with the coarse-grained area seen in aerial photographs to the northwest, the area with similarly resistive deposits near the end of lines 10 and 3, and the area at the beginning of line 7 (fig. 2). Line 2 intersected line 10 (fig. 2) approximately 27 m from the beginning of the profile.

Line 10

Line 10 data (fig. 10) were collected south to north, parallel to crop rows in August 2013. The line crossed the visible channel deposits at an acute oblique angle (fig. 2). The maximum thickness of sand deposits along this line was interpreted on the basis of the same resistivity value that corresponded to the bottom of sand in line 2. A line was drawn to approximate the area of these deposits by projecting the lowest elevation of the 220 ohm-m resistivity contour to the trace of the channel deposits visible at land surface in aerial photographs. Line 10 intersected line 2 and line 7 (fig. 2). Because of the acutely oblique angle of the line, the cross-sectional area of the channel deposits was not directly comparable to that measured along line 2 (fig. 9), which was oriented nearly perpendicular to the channel. However, line 10 showed the variation of channel thickness sub-parallel to the channel axis, improving understanding of the geometry of channel deposits in three dimensions. The thickest channel deposits were encountered between 28 and 56 m and had a thickness of 4 to 6 m.

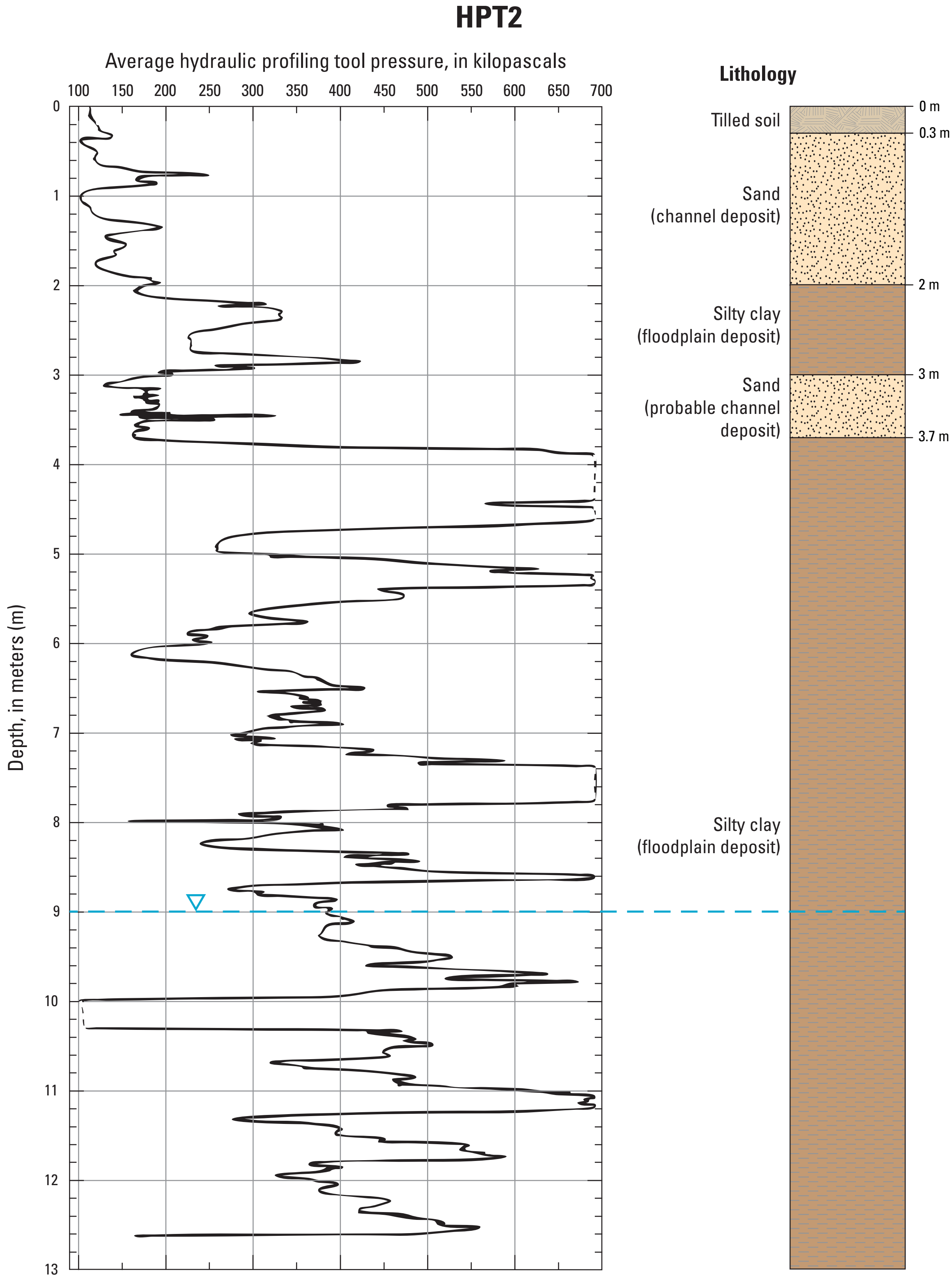

Figure 8. Vertical profile HPT2 generated by hydraulic profiling tool in field 1 (fig. 2) and interpreted lithology, abandoned channel next to the San Joaquin River, Merced County, California, 2013. Dashed line in hydraulic profiling tool profile indicates where measurement exceeded instrument threshold. Data correlates with 24 meters on line 2.

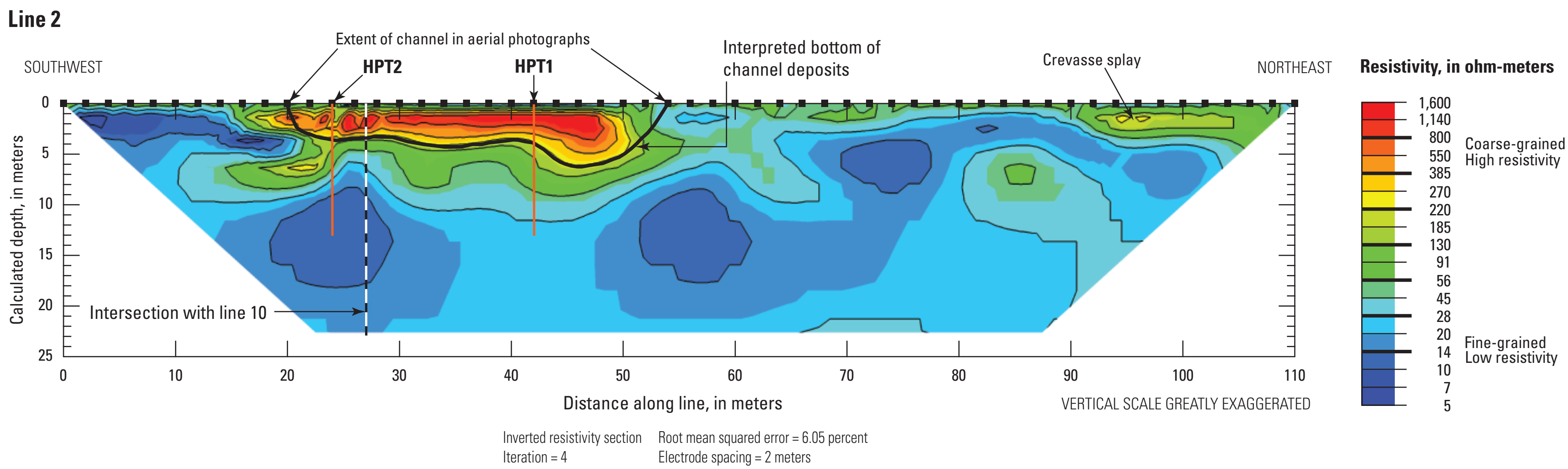

Figure 9. Modeled direct-current resistivity data collected along line 2, abandoned channel near the San Joaquin River, Merced County, California, 2012. See figure 2 for line location.

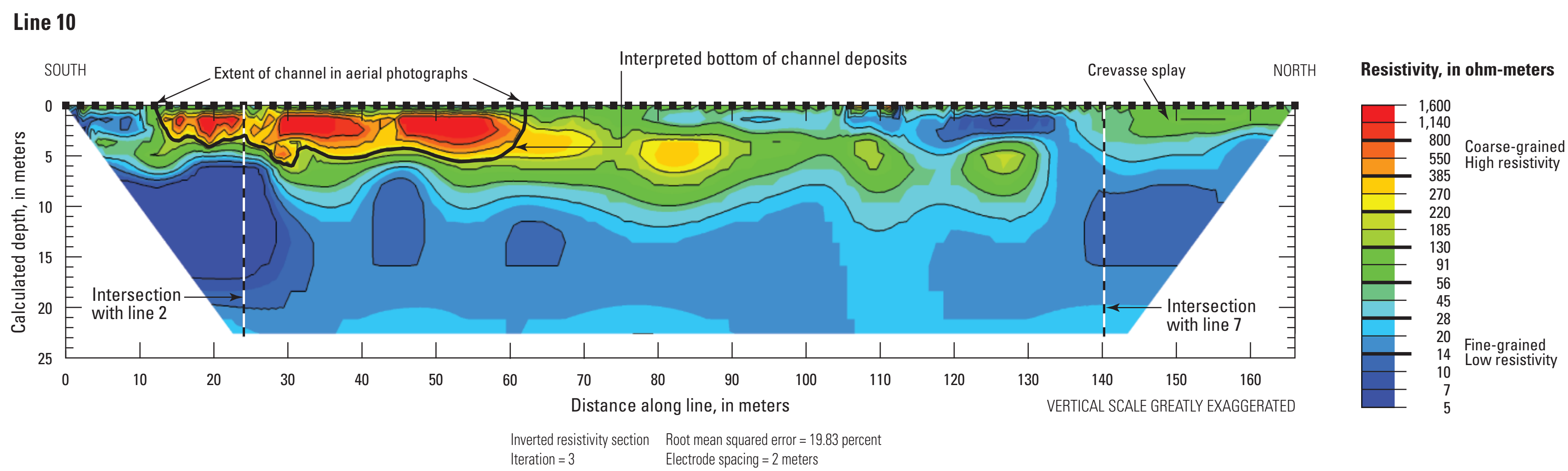

Figure 10. Modeled direct-current resistivity data collected along line 10, abandoned channel near the San Joaquin River, Merced County, California, 2013. See figure 2 for line location.

A moderately resistive zone near the northern end of the profile correlated with the thin, shallow deposits observed at the end of lines 2 (fig. 9) and 3 and at the beginning of line 7. These deposits are likely to be a crevasse splay composed of a mixture of silt, sand, and gravel, based on their geometry (Boggs, 2006).

Line 3

Line 3 (fig. 11) was approximately 120 m northwest of line 2, along the same abandoned meander, farther from the active channel of the San Joaquin River. Line 3 data were collected perpendicular to the channel axis as identified in aerial photographs (fig. 2). Although the starting points (0 m) of lines 2 and 3 were only offset by 124 m, the width of the channel decreased by about 40 percent from line 2 to line 3. The channel deposits at line 3 were about 22-m wide and were visible at land surface between 22 and 42 m. Along line 3, the channel deposits were thickest between 32 and 36 m, extending to a depth of about 4 m.

The modeled data along line 3 showed high resistivity in the shallow subsurface across a slightly wider area (from 18 to 42 m) than the sand channel indicated by the aerial photographs. The resistive unit is present below 2-m-depth southwest of the end of the surface expression of the channel at 22 m, and a moderately resistive feature persisted to the edge of the model.

A near-surface moderately resistive zone visible from 80 m to the end of the line at 110 m, and less than 2 m thick, is likely composed of crevasse splay deposits. This moderately resistive zone was observed in aerial photographs to be sandy sediment, and can be traced at the east ends of lines 2 and 10 and at the west end of line 7. An additional feature of moderate resistivity (green) was below 7 m depth at the east end of line 3; this feature directly below the crevasse splay could indicate a hydraulic connection between the river and fields.

Line 12

Line 12 data (fig. 12) were collected south to north, parallel to crop rows, in August 2013. The line was nearly perpendicular to the channel deposits, which are between 62 and 88 m in the aerial photographs (fig. 2). The inside of the abandoned meander is the south side of the visible channel deposits, where the thickest high-resistivity units are measured. The interpreted bottom of the sandy deposits was projected from the lowest elevation of the 220 ohm-m contour to where the channel deposits pinch out at land surface. Another discrete unit of moderate-to-high resistivity, not visible in aerial photos, was below 3-m depth between 108 and 120 m, north of the visible channel. This unit could be a small abandoned channel or crevasse splay that was buried by a later flooding event.

Line 4

Near the northern margin of field 1, line 4 data (fig. 13) were collected somewhat obliquely to the trace of the channel deposits observed in the aerial photographs (fig. 2). The channel deposits were visible at land surface in the aerial photographs between 74 and 110 m. Line 4 was in a relatively straight reach of the channel deposits, and the thickest deposits were in the middle of the channel. The channel deposits in this model extended from the deepest 220 ohm-m contour projected to the surface from 78 to 110 m, which was less than the width of the channel deposits in the aerial photographs (fig. 2). The width of the channel measured from aerial photographs was correctly estimated by moderate resistivity units (100–200 ohm-m) that still stand in contrast to the low-resistivity flood plain deposits (less than 50 ohm-m), however. Sand from the channel deposits could have been redistributed on the surface by agricultural practices, and could have resulted in the difference between the channel width seen in the resistivity data compared to the aerial photographs. The sediments represented by the 100–200 ohm-m unit could be capable of transmitting a large flow, if saturated.

Line 7—Cross-Canal Field 1

Line 7 (fig. 14) was collected perpendicular to the axis of the active channel of the San Joaquin River. Line 7 began in field 1, crossed the irrigation canal, and ended on a point-bar deposit on the inside of a meander of the active channel. This line crossed lines 10 and 6 (fig. 2).

A moderate-to-high resistivity (100–200 ohm-m) unit was present in the shallow subsurface from 6 to 23 m. This unit was also measured on line 2 (fig. 9), line 3 (fig. 11), and line 10 (fig. 10) and could be composed of thin, relatively sandy, crevasse splay deposits. Another area of moderate resistivity (less than 185 ohm-m) was present from 3 to 5 m depth between 50 to 60 m and could represent a sandy deposit.

The unlined earthen irrigation canal was present as a low resistivity zone (less than 30 ohm-m) between 74 m and 82 m that extended from the ground surface to at least 4 m depth. Although the depth of the water in the canals was less than 2 m in June 2013, when these data were collected, the extension of this low-resistivity zone beneath the bottom of the canal could be due to leakage of canal water saturating the underlying sediment. On the northeast end of line 7, the point-bar deposits of the San Joaquin River were measured as a high-resistivity unit (greater than 500 ohm-m). The contours at the margins of this unit were closely spaced, indicating a sharp contrast between materials of different electrical properties. The plunging trend of the contours indicated a large resistive unit (or shadow effect of this unit) was present beyond the end of the resistivity line. Because this feature was near the end of the line, its true thickness and the extent of its shadow effect could not be determined from the resistivity data alone. Field observations indicated the sandy bank of the point-bar deposit at this location was greater than 5-m thick (fig. 15). Excavation into the side of the bank approximately 2 m below the top of the bank revealed (fig. 16) thick, cross-bedded sand deposits composing the point-bar deposits near the east end of line 7.

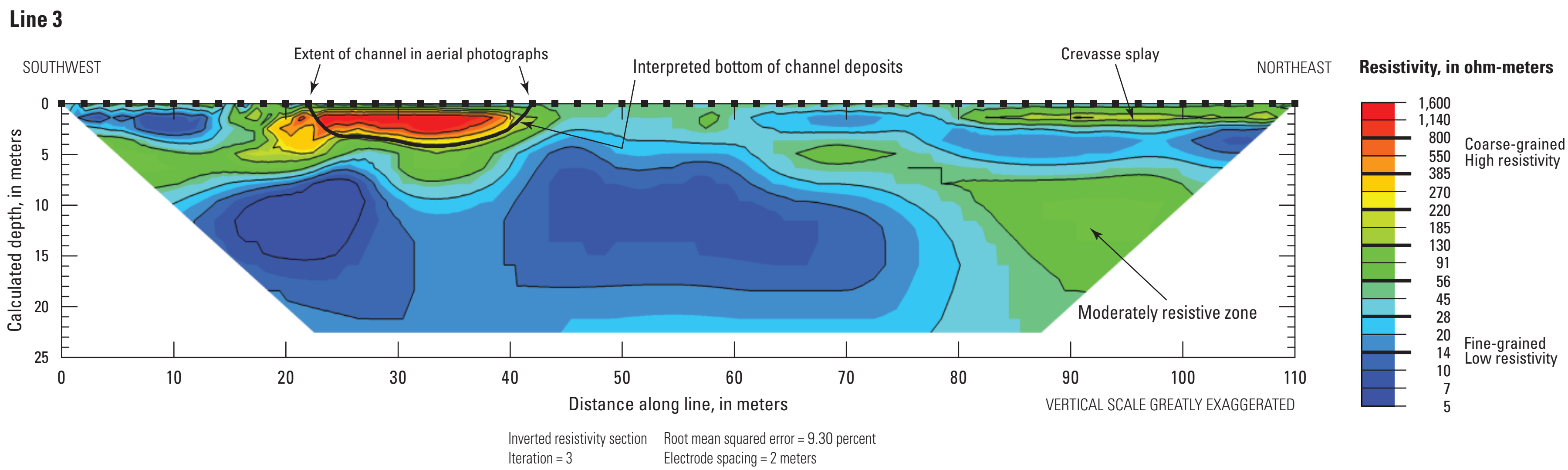

Figure 11. Modeled direct-current resistivity data collected along line 3, abandoned channel near the San Joaquin River, Merced County, California, 2012. See figure 2 for line location.

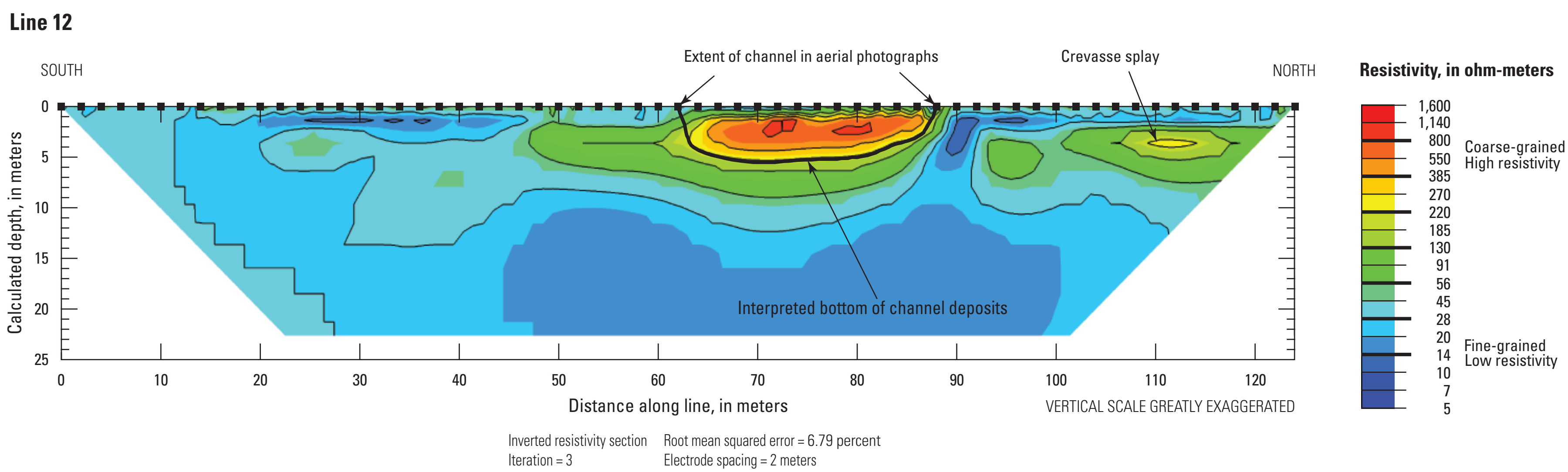

Figure 12. Modeled direct-current resistivity data collected along line 12, abandoned channel near the San Joaquin River, Merced County, California, 2013. See figure 2 for line location.

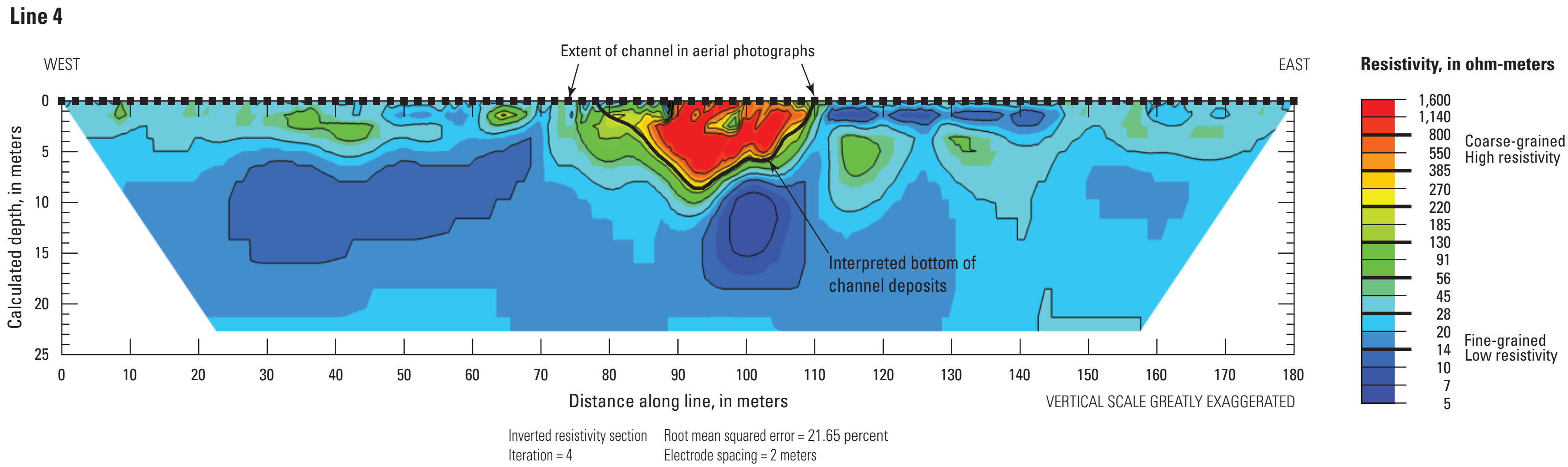

Figure 13. Modeled direct-current resistivity data collected along line 4, abandoned channel near the San Joaquin River, Merced County, California, 2012. See figure 2 for line location.

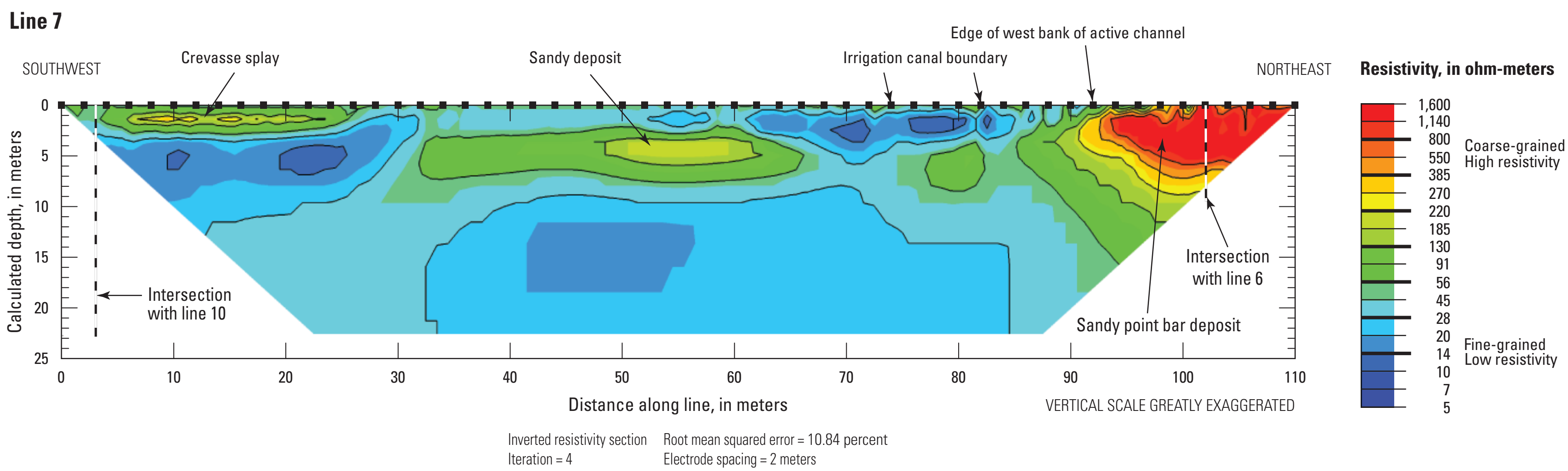

Figure 14. Modeled direct-current resistivity data collected along line 7, field 1 near the San Joaquin River, Merced County, California, 2013. See figure 2 for line location.

Figure 15. Sandy bank of a point-bar deposit along the northeast end of line 7 (figs. 2, 14) in the San Joaquin River, Merced County, California, 2013.

Figure 16. Excavation into river bank at a point-bar deposit along the northeast end of line 7 (figs. 2, 14) in the San Joaquin River, Merced County, California, 2013.

Field 2

Field 2 was the smallest field investigated during the course of this study. The field is bounded by field 1 to the south and west, and the irrigation canal and San Joaquin River to the north and east. An abandoned channel splits into two branches at the southern edge of the field (fig. 2). Both branches of the abandoned channel appear smaller in cross-sectional area than the channels in fields 1 and 3. Two direct-current resistivity lines were collected in field 2.

Line 1

Line 1 was in field 2, northeast of the main abandoned channel described in the “Field 1” section of this report. The inverted resistivity pseudosection along this profile is shown in figure 17. The abandoned channel in field 2 was substantially narrower than the channel identified in field 1. Line 1 data showed a moderately resistive unit (greater than 50 ohm-m) less than 2-m thick beneath the channel identified in aerial photographs (46–70 m). Auger holes confirmed that a textural contrast exists between the channel, its bank, and underlying deposits, and the channel is composed of sediment with texture similar to that observed in the resistivity profile from line 2 (A.M. Warren, Bureau of Reclamation, written commun., January 25, 2013). The subdued resistivity values at line 1 (at least several hundred ohm-m lower than those at line 2), in-part, could be a function of the difference in the thicknesses of the deposits between line 1 (less than 2 m) and line 2 (6 m). Because of the redistribution of fine-grained surficial deposits associated with the plowing and flood-irrigation practices at this site, the upper 0.3 m of the subsurface, which included noticeable silts and clays, made up a greater percentage of the cross-sectional area of the abandoned channel at line 1 than at line 2. The modeling and inversion process may have averaged the high resistivity measured in the abandoned channel with the low resistivity of the overlying soil and underlying floodplain, which effectively lowered the measured apparent resistivity of the moderate resistivity feature along line 1. Similar near-surface features are also seen at lines 2 (fig. 9), 10 (fig. 10), 3 (fig. 11), and 7 (fig. 14). These features, which display similar resistivity values and are also less than 3-m thick, could be interpreted as crevasse splay deposits rather than abandoned meanders.

Line 8—Cross-Canal Field 2

Line 8 data (fig. 18) were collected perpendicular to the axis of the irrigation canal. Line 8 began in field 2, crossed the irrigation canal, and ended on a point-bar deposit on the inside of a meander of the active channel (fig. 2). A relatively large, moderately resistive zone extends from 4 to 7 m below land surface and from 22 m to 56 m along line 8. This moderately resistive zone could be composed of relatively coarse-grained sandy sediment. The irrigation canal was between 70 m and 80 m and appeared in the resistivity line as a zone of low-resistivity values (less than 30 ohm-m). The section of the resistivity profile beneath the irrigation canal had a very low resistivity extending to nearly 4 m below land surface. This low resistivity zone, in-part, could reflect leakage from the overlying earthen irrigation canal. Saturation of underlying sediment could have suppressed any highly resistive signals from coarse-grained deposits directly underlying the canal.

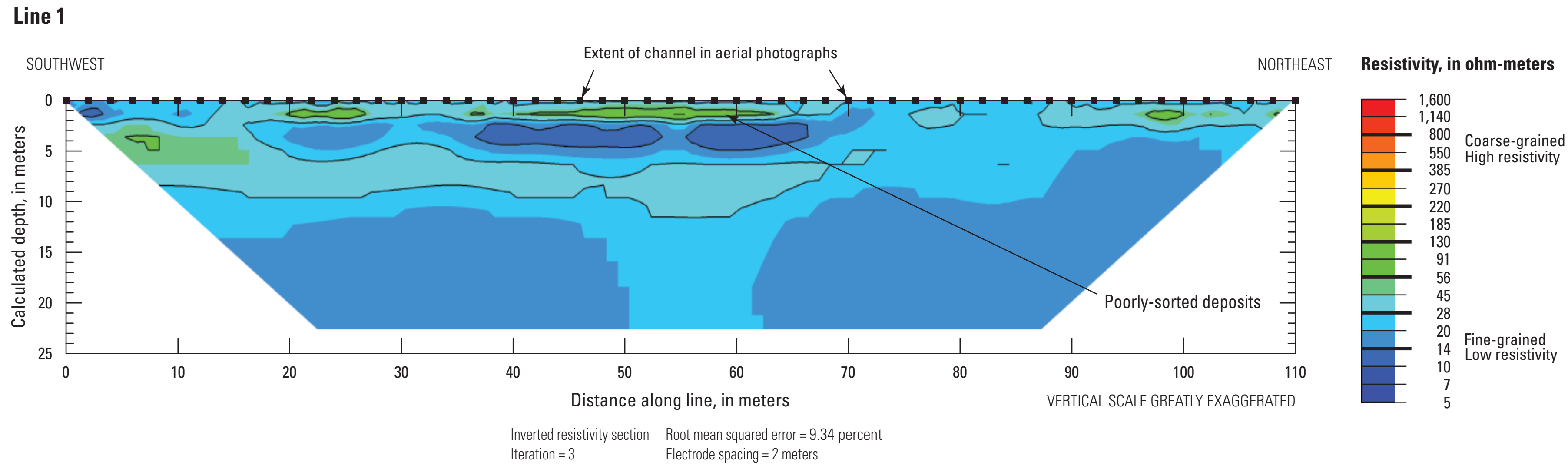

Figure 17. Modeled direct-current resistivity data collected along line 1, field 2 near the San Joaquin River, Merced County, California, 2012. See figure 2 for line location.

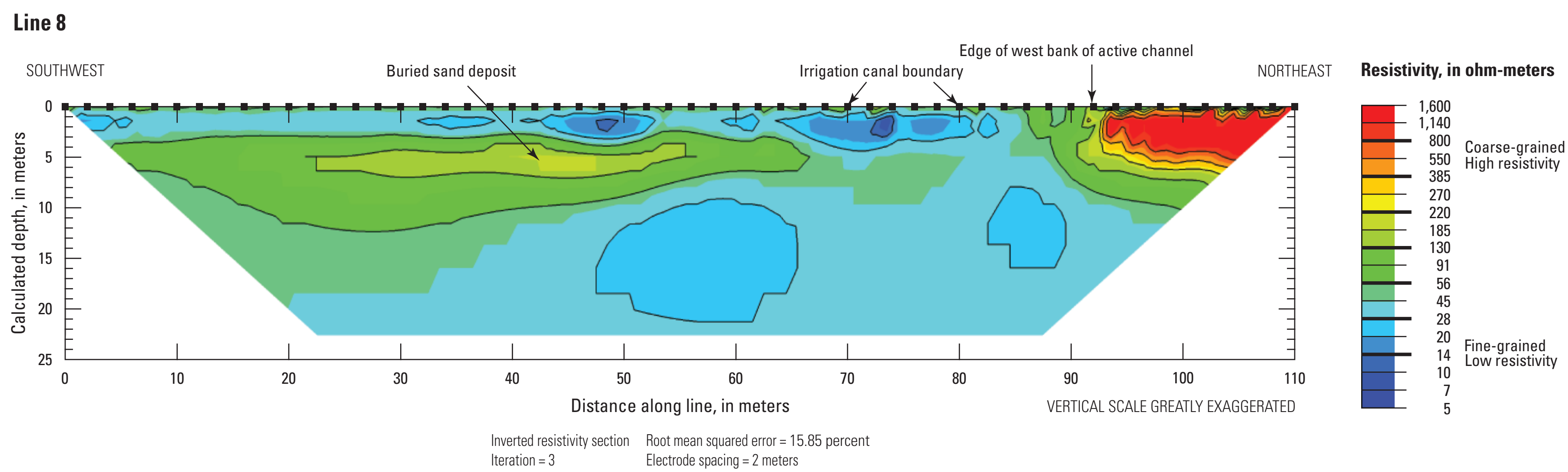

Figure 18. Modeled direct-current resistivity data collected along line 8, field 2 near the San Joaquin River, Merced County, California, 2013. See figure 2 for line location.

Across the irrigation canal, starting at 92 m, the point-bar deposits of the active river channel appeared as a high resistivity unit (greater than 500 ohm-m). The contours at the margins of this unit were closely spaced, indicating a sharp contrast between materials of different electrical properties. The plunging trend of the contours indicated that a larger resistive body is present northeast of the resistivity line. These resistive point-bar deposits were similar in resistivity and shape to those measured on line 7 (fig. 14).

Field 3

Field 3, the southernmost of the three fields investigated in this study, parallels field 1, although field 3 is slightly smaller in area. Field 3 intersects the San Joaquin River at the southeastern edge of the field. The trace of an abandoned channel is visible from the edge of field 3 at the San Joaquin River, across the length of field 3, and into the next field to the northwest, outside of the study area (fig. 2). Two direct-current resistivity lines were collected in this field.

Line 11

Line 11 data (fig. 19) were collected from southwest to northeast across the trace of the abandoned channel in field 3 (fig. 2). This line was farther from the active channel than the other resistivity profiles collected during this study. The abandoned channel crossed line 11 between 24 and 46 m and reached a maximum depth of approximately 10 m, based on the 220 ohm-m resistivity contour. This channel can be traced in aerial photographs to the southeast through the agricultural field to its intersection with the active channel of the San Joaquin River. This intersection is discussed in more detail later in this report in the subsection on line 9.

There is a moderate-to-high resistivity zone at a depth of 3.5 to 6 m near the northeast end of the profile between 82 m and 98 m. There is little-to-no trace of this resistive zone at land surface, but the similarities in subsurface geometry and modeled resistivity values of this zone to the thin, shallow deposits in field 1 indicate that this resistive zone could be a buried crevasse splay. A moderately resistive zone (between 56 and 185 ohm-m) connects the abandoned channel between 24 m and 46 m to these possible crevasse splay deposits. If the zone centered beneath 92 m is a crevasse splay, then the moderately resistive zone connecting to it could be a mixture of silt and sand. Further investigation is required to confirm the texture and potential connection between the crevasse splay and abandoned channel.

Line 9—Cross-Canal Field 3

Line 9 data (fig. 20) were collected perpendicular to the axis of the active channel of the San Joaquin River. It began near the trace of the abandoned meander in field 3, crossed the irrigation canal, and ended in coarse-grained deposits (which may have been a former point bar) on the outside of a meander in the active channel (fig. 2). This line crossed the abandoned channel at an acutely oblique angle to the axis of the abandoned channel. This line was collected to investigate the potential for a hydraulic connection between the abandoned channel in field 3 and the active San Joaquin River at this location.

The trace of the abandoned channel measured in line 9 began near 18 m and can be traced along the profile beyond the intersection with the irrigation canal (72 m). The irrigation canal was between 72 m and 80 m and appeared on line 9 as a zone of low resistivity (less than 30 ohm-m) near the surface. The deposits directly below the irrigation canal appeared as a zone of moderate resistivity; these deposits could actually be composed of coarse sediment that was partially saturated as a result of leakage from the overlying unlined earthen canal. There was a cut bank of the active channel consisting of a clean, medium sand at the southeast end of the profile (fig. 21). The slope of this cut bank is gradual from the levee road to the river bed, in contrast to field observations of vertical cut-banks in silty deposits. The surficial trace of the sand that composes the active-channel margin can be seen in line 9 as a zone of moderately high resistivity (greater than 200 ohm-m) near the surface between 104 and 110 m, at the end of the resistivity line.

Inspection of line 9 revealed that the medium sand of the active river bank could have been partially buried during construction of the irrigation canal. Sand deposits can be traced in the subsurface from the channel margin, underneath the irrigation canal, and into the agricultural field. If canal water infiltration caused the lower resistivity beneath the canal, in what is probably a homogenous sandy deposit, then this profile shows that the abandoned channel in field 3 is probably lithologically connected to the sand deposits that compose the active channel margin. If the water table rises in response to higher stream stages, a hydraulic connection of saturated sandy deposits in the subsurface from the active channel into the agricultural field could result.

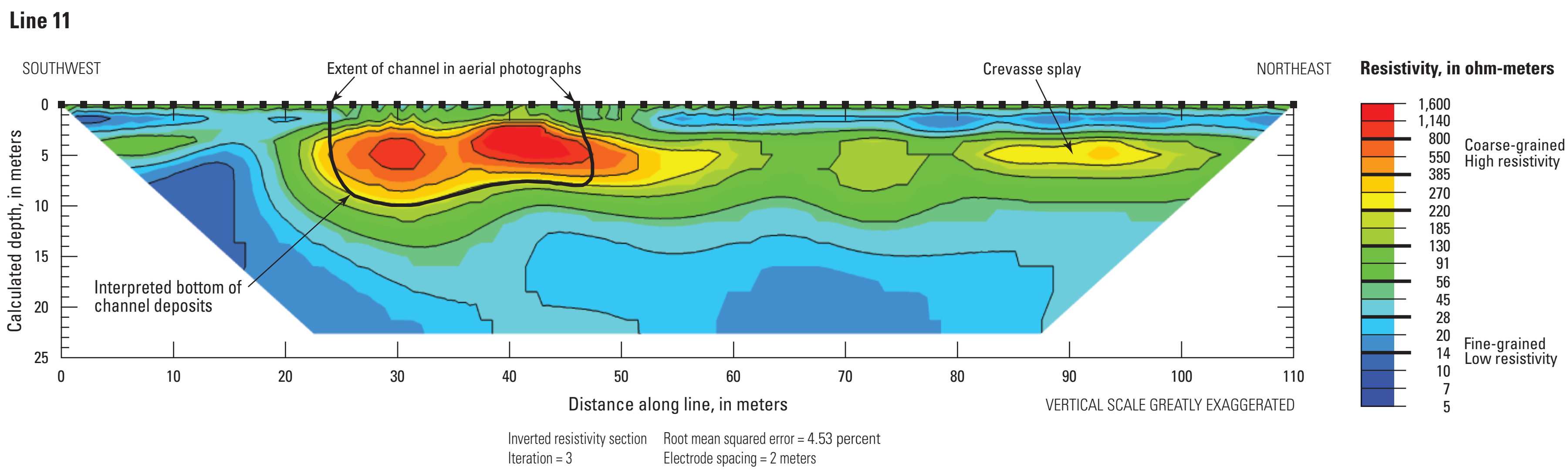

Figure 19. Modeled direct-current resistivity data collected along line 11, abandoned channel near the San Joaquin River, Merced County, California, 2013. See figure 2 for line location.

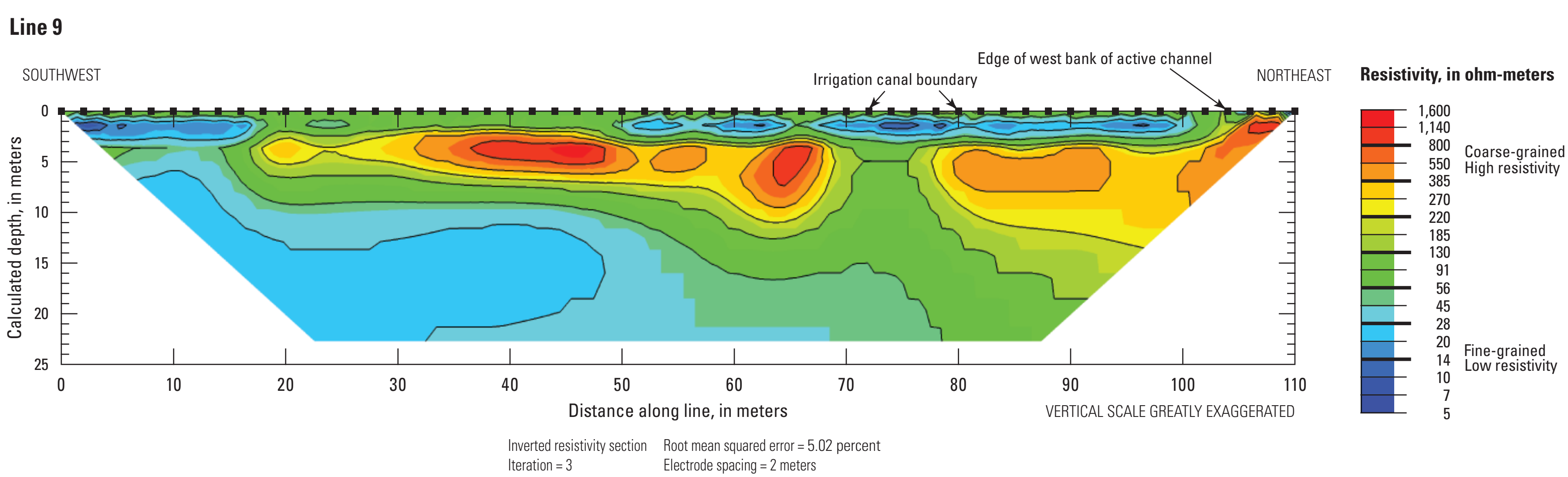

Figure 20. Modeled direct-current resistivity data collected along line 9, field 3 near the San Joaquin River, Merced County, California, 2013. See figure 2 for line location.

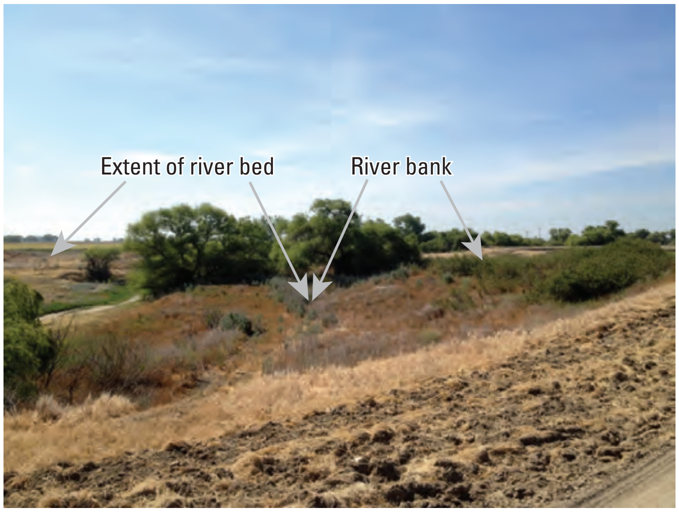

Figure 21. West bank of the San Joaquin River, east of line 9 (fig. 20), Merced County, California. Photo was taken from the levee road and is looking south. Brush covered slope in the center right of the photo is the river bank. See figure 2 for location of line 9.

Electrical Resistivity Investigation of the Active Channel and its Banks

Two resistivity lines were collected in the active San Joaquin River channel to investigate if potential seepage conduits were present in the banks or directly beneath the dry channel. Both lines presented in this section were collected east of field 1 (fig. 2).

Line 5—River Bed

Line 5 (fig. 22) was collected in the bed of the active San Joaquin River during a no-flow period in May 2013 (fig. 2). Line 5, which was southeast of line 6, was collected sub-parallel to the axis of the active channel. A zone of high resistivity was present in the near-surface between 76 m to 98 m. This resistive zone was 28 m directly east of the southern end of line 6 and could represent coarse-grained deposits.

There was a zone of moderate resistivity present at depths below 7 m and extending from 62 m to 74 m. This zone is likely to have been saturated and could have a coarser texture than the surrounding sediments. Of particular note is the lack of an extensive high-resistivity body beneath the river bed in this location that could act as a direct conduit for seepage through the river bed during increased flows. Other than the moderately resistive zone centered beneath 66 m, this line showed that the subsurface beneath the scoured active channel was either moist or composed of fine-grained sediment at this location. Because this line was collected at an elevation approximately 6 m lower than those of the fields, the water table was closer to land surface than in other sections, and features were harder to resolve in the thinner unsaturated zone.

Line 6—Chute Channel on a Point-Bar Deposit

Line 6 (fig. 23) was collected by using a 1-m electrode spacing parallel to the axis of a chute channel (fig. 24) on a point-bar deposit in the active San Joaquin River channel (fig. 2). Although the fit of the model to the data for this line was of much poorer quality (51.3 percent root mean squared error, RMSE) than other lines (average RMSE was 11.0 percent), in part because of the high contact resistances measured here, the model indicated highly resistive point-bar deposits to an apparent depth of at least 9.5 m. The high resistivity of this dry, sandy point-bar deposit had a similar effect on the data acquisition process as the shadow effect described in discussing line 2, where the resistivity of the subsurface was high enough to block the passage of current between electrodes, inhibiting accurate readings below the high-resistivity layer. Consequently, the distribution of resistivity beneath the near-surface high resistivity layer is uncertain.

Line 6 intersected with line 7 (figs. 2, 14) at a 90-degree angle near 21 m. The resistive body at the northeastern end of line 7 extended to a minimum depth of 8.5 m. A 2-m-deep excavation near the northeastern end of line 7 penetrated cross-bedded sand (fig. 16).

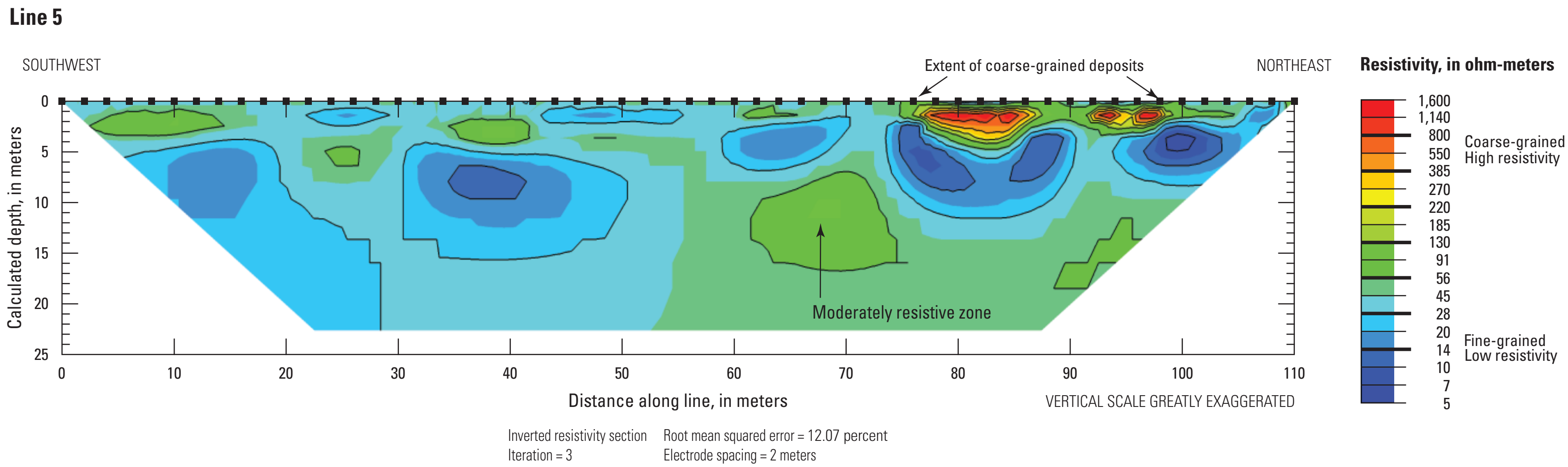

Figure 22. Modeled direct-current resistivity data collected along line 5 in the (dry) San Joaquin River, Merced County, California, 2013. See figure 2 for line location.

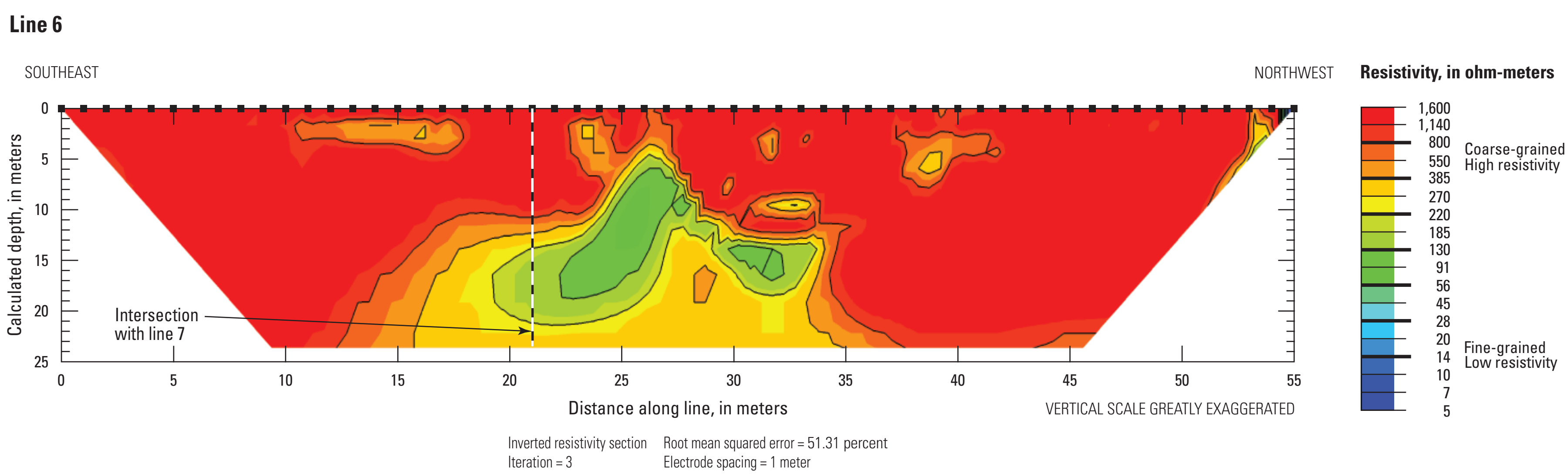

Figure 23. Modeled direct-current resistivity data collected along line 6, west bank of the San Joaquin River, Merced County, California, 2013. See figure 2 for line location.

Figure 24. View to the northwest along a sandy surface of a chute channel, San Joaquin River, Merced County, California. Area of figures 15 and 16 is the slope to the right of this photo.

Study Limitations

The 2D modeling of a three-dimensional (3D) environment has inherent errors. Because many of the curvilinear features of fluvial deposits (for example, contacts between deposits, units that pinch out) are 3D, there is uncertainty in the resistivity results when 3D structures cannot be explained in 2D. For example, there is loss of energy as electrical fields bend around the contact between floodplain and channel deposits along curves of a meander (for example, where line 12 crosses the tight arc of the meander, possibly) that can result in false, overly resistive readings. Features such as this may have resulted in noisy data and relatively high root mean square errors (RMSE) for some resistivity profiles. The 2D modeling of direct-current resistivity data is a common approach, however, and the inherent errors are accepted because there is no way to nullify these effects, and valuable subsurface information can still be obtained despite these limitations.

The modeled pseudosections did not represent the true spatial distribution of resistivity values in the subsurface. This is because the diffusive nature of energy propagation in electrical sounding experiments cannot resolve sharp boundaries (Constable and others, 1987). For example, a shadow effect (Kuznetzov, 1982; Zonge and Hughes, 1988) beneath the channel deposits in line 2 masks the true resistivity of the subsurface because of ground-wave distortion relative to a uniform half-space (Yan and Fu, 2004). This phenomena has been documented in other electrical geophysical methods (controlled-source audio frequency magnetotellurics) and has been simulated by numerical modeling (Newman and others, 1986; Zonge and others, 1986; Mitsuhata, 2000). When anomalies such as geologic contacts are present between the transmitter and receiver, the measured data can be distorted so that the geological structure will not be inferred correctly (Yan and Fu, 2004). As a result, the modeled data do not represent the true spatial distribution of resistivity values in the subsurface. Lithologic data from hand auger and core samples provided a method of correlating modeled DC resistivity data with subsurface conditions in the study area.

There is uncertainty about the relative values of resistivity among lines collected at different times because pore-water saturation and water-table depth could have changed. Other than the contact resistance tests collected prior to data acquisition, results of which were consistently less than 1.0 kohm-m in floodplain deposits in all field campaigns, there were no data on the moisture conditions in the soils. The errors that could result from this uncertainty can be large, but because of the wide spread in the resistivity values between different deposits, interpretations of the distributions of larger lithologic features are likely to be robust. Where features of moderate resistivity values (between 50 and 200 ohm-m) are described, there is uncertainty regarding whether lithology, soil moisture, or a combination of variables contributed to the presence of anomalies in the data.

Summary and Conclusions

Increased flows in the San Joaquin River, part of the San Joaquin River Restoration Program, are designed to help restore fish populations. However, increased seepage losses could result from these higher restoration flows, which could exacerbate existing drainage problems in neighboring agricultural lands and potentially damage crops. Channel deposits of abandoned river meanders that are hydraulically connected to the river could act as seepage conduits, allowing rapid and widespread water-table rise during restoration flows. There is a need to identify the geometry and properties of these channel deposits to assess their role in potential increased seepage effects and to evaluate management alternatives for reducing seepage. Three agricultural fields with abandoned channels visible in aerial photographs were selected along Reach 4A of the San Joaquin River. The Bureau of Reclamation partnered with the U.S. Geological Survey to study abandoned channel deposits in the three fields using electrical and electromagnetic geophysical methods.

The purpose of this report is to present interpreted direct-current resistivity data from surveys that were done in agricultural fields near the active channel of the San Joaquin River. Abandoned river channels in three fields were investigated to evaluate the textural and morphological differences between the channels and surrounding overbank deposits, and assess the potential hydraulic connection between the abandoned meanders and the active channel of the San Joaquin River. Interpretation of the geophysical data was constrained by several types of independent data, including analyses of collected cores, hand-auger samples, direct-push hydraulic profiling tool (HPT) logs, and aerial photographs.

The inverted resistivity profiles indicated that the direct-current (DC) resistivity method was able to differentiate between coarse- and fine-grained fluvial deposits. The stark variations in resistivity observed in the models interpreted in this report were primarily a function of the contrasts in electrical properties between coarse-grained channel deposits and fine-grained floodplain deposits, and not of large variations in saturation or the detection of the top of the water table.

Some uncertainties in the interpretation of the inverse resistivity models involved uncertain water content in the unsaturated zone over time from irrigation and precipitation and the influence of shadow effects beneath thick, coarse-grained/high-resistivity deposits. Numerous fluvial landforms, including point-bar deposits, channel deposits, floodplain deposits, and crevasse splays, were identified and differentiated in the study area. The ability to recognize a lithologic connection between the river and abandoned channels, and resultant hydraulic connection during increased flows, was a key finding. This was demonstrated at the abandoned channel in field 3 that appeared to be lithologically connected to the sand deposits that compose the active channel margin.

The DC resistivity data differentiated coarse- and fine-grained fluvial deposits of the San Joaquin River system and enabled mapping of these units through the subsurface. Nested within fine-grained floodplain deposits, coarse-grained deposits in abandoned meanders extend from, or near, land surface in the agricultural fields to depths of 4 to 10 meters. These coarse-grained deposits could provide highly conductive hydraulic conduits extending the entire length of their sinuous traces through the agricultural land investigated in this study. In particular, resistivity profiles crossing the channel in the southernmost agricultural field (field 3) revealed that the sandy deposits of the abandoned channel are likely to be lithologically connected to the sandy bank of the active San Joaquin River channel. During periods of elevated flow in the river, water could seep laterally through the bank of the channel, raising the water table, and allowing direct movement of seepage into the shallow subsurface of the neighboring agricultural field, potentially causing damage to crops. Additionally, an anomaly of moderate resistivity below 7 meters at the east end of line 3 could indicate another hydraulic connection between the river and agricultural fields.

Although DC resistivity proved to be effective at identifying and mapping the depths of these abandoned channels in two dimensions, the labor-intensive method is limited in the amount of ground that can be covered. For this reason, other geophysical methods, such as frequency domain electromagnetics or a capacitively coupled resistivity meter, could be more effective at mapping the electrical properties of the three agricultural fields in Reach 4A and at sites along other reaches of the San Joaquin River to determine hydraulic conductivity distributions to use as input to groundwater models.

References Cited

Advanced Geosciences Inc., 2009, Instruction manual for EarthImager 2D, version 2.4.0—Resistivity and IP inversion software: Austin, Texas, 139 p.

Advanced Geosciences Inc., 2011, The SuperSting with swift automatic resistivity and IP system instruction manual: Austin, Texas, 105 p.

Archie, G.E., 1942, The electrical resistivity log as an aid in determining some reservoir characteristics: Transactions of the American Institute of Mining Metallurgical and Petroleum Engineers, v. 146, p. 54–62.

Bersezio, R., Giudici, M., and Mele, M., 2007, Combining sedimentological and geophysical data for high-resolution 3-D mapping of fluvial architectural elements in the Quaternary Po plain (Italy): Sedimentary Geology, v. 202, p. 230–248.

Biella, G., Lozej, A., and Tabacco, I., 1983, Experimental study of some hydrogeophysical properties of unconsolidated porous media: Ground Water, v. 21, no. 6, p. 741–751.

Binley, A., and Kenma, A., 2005, DC resistivity and induced polarization methods, *in* Rubin, Y., and Hubbard, S.S., eds., Hydrogeophysics: Dordrecht, Netherlands, Springer, p. 129–156.

Boggs, S., Jr., 2006, Principles of sedimentology and stratigraphy (4th ed.): Upper Saddle River, N.J., Pearson Prentice Hall, 662 p.

Bowling, J.C., Harry, D.L., Rodriguez, A.B., and Zheng, C., 2006, Integrated geophysical and geological investigation of a heterogeneous fluvial aquifer in Columbus, Mississippi: Journal of Applied Geophysics, v. 62, p. 58–73.

Brosten, T.R., Day-Lewis, F.D., Schultz, G.M., Curtis, G.P., and Lane, J.W., Jr., 2011, Inversion of multi-frequency electromagnetic induction data for 3D characterization of hydraulic conductivity: Journal of Applied Geophysics, v. 73, p. 323–335.

Callegary, J.B., Leenhouts, J.M., Paretti, N.V., and Jones, C.A., 2007, Rapid estimation of recharge potential in ephemeral stream channels using electromagnetic methods, and measurements of channel and vegetation characteristics: Journal of Hydrology, v. 73, p. 323–335.

Cardenas, M.B., and Markowski, M.S., 2011, Geoelectrical imaging of hyporheic exchange and mixing of river water and groundwater in a large regulated river: Environmental Science and Technology, v. 45, p. 1407–1411.

Constable, S.C., Parker, R.L., Constable, C.G., 1987, Occam's inversion—A practical algorithm for generating smooth models from electromagnetic sounding data: Geophysics, v. 52, no. 3, p. 289–300.

Easterbrook, D.J., 1993, Surface processes and landforms: New York, MacMillan Publishing Company, 520 p.

Froese, D.G., Smith, D.G., and Clement, D.T., 2005, Characterizing large river history with shallow geophysics—Middle Yukon River, Yukon Territory and Alaska: Geomorphology, v. 67, p. 391–406.

Furman, A., Ferré, T.P.A., and Warrick, A.W., 2003, A sensitivity analysis of electrical resistivity tomography array types using analytical element modeling: Vadose Zone Journal, v. 2, p. 416–423.

Keller, G.V., and Frischknecht, F.C., 1966, Electrical methods in geophysical prospecting: Oxford, England, Pergamon Press, 519 p.

Kuznetzov, A.N., 1982, Distorting effects during electromagnetic sounding of horizontally nonuniform media using an artificial field source: Earth Physics, v. 18, p. 130–137.

Kwader, T., 1985, Estimating aquifer permeability from formation resistivity factors: Ground Water, v. 23, no. 6, p. 762–766.

McBain and Trush, Inc., 2002, San Joaquin River restoration study background report: Friant Water Users Authority and Natural Resources Defense Council, 1055 p. http://www.waterboards.ca.gov/waterrights/water_issues/programs/bay_delta/bay_delta_plan/water_quality_control_planning/docs/sjrf_spprtinfo/mcbainandtrush_2002.pdf.

McCall, W., Nielsen, D.M., Farrington, S., Christy, T.M., 2009, Application of direct push methods to investigate uranium distribution in an alluvial aquifer: Ground Water Monitoring and Remediation, v. 29, no. 4, p. 65–76.

Minsley, B.J., Ball, L.B., Caine, J.S., Curry-Elrod, E., and Manning, A.H., 2010, Geophysical characterization of subsurface properties relevant to the hydrology of the Standard Mine in Elk Basin, Colorado: U.S. Geological Survey Open-File Report 2009–1284, 46 p.

Minsley, B.J., Smith, B.D., Hammack, R., Sams, J.I., and Veloski, G., 2012, Calibration and filtering strategies for frequency domain electromagnetic data: Journal of Applied Geophysics, v. 80, p. 56–66.

Mitsuhata, Y., 2000, 2-D Electromagnetic modeling by finite-element method with a dipole source and topography: Geophysics, v. 65, p. 465–475.

Moore, D.M., and Reynolds, R.C., 1997, X-ray diffraction and the identification and analysis of clay minerals: New York, Oxford University Press, 378 p.

Mount, J.F., 1995, California rivers and streams: Berkeley, University of California Press, 359 p.

Newman, G.A., Hohmann, G.W., and Anderson, W.L., 1986, Transient electromagnetic response of three-dimensional bodies in a layered earth: Geophysics, v. 51, p. 1608–1627.

Nyquist, J.E., Freyer, P.A., and Toran, L., 2008, Stream bottom resistivity tomography to map ground water discharge: Ground Water, v. 46, no. 4, p. 561–569.

Reynolds, J.M., 1997, An introduction to applied and environmental geophysics: Chichester, England, John Wiley & Sons, 796 p.

Telford, W.M., Geldart, L.P., and Sheriff, R.E., 1990, Applied geophysics (2nd ed.): New York, Cambridge University Press, 770 p.

Wojnar, A.J., Mutiti, S., and Levy, J., 2013, Assessment of geophysical surveys as a tool to estimate riverbed hydraulic conductivity: Journal of Hydrology, v. 482, p. 40–56.

Yan, S., and Fu, J., 2004, An analytical method to estimate shadow and source overprint effects in CSAMT sounding: Geophysics, v. 69, no. 1, p. 161–163.

Zeleke, T.B., and Si, B.C., 2005, Scaling relationships between saturated hydraulic conductivity and soil physical properties: Soil Science Society of America Journal, v. 69, p. 1691–1702.

Zonge, K.L., Ostrander, A.G., and Emer, D.F., 1986, Controlled source audio-frequency magnetotelluric measurements, *in* Vozoff, K., ed., Magnetotelluric methods: Tulsa, Okla., Society of Exploration Geophysicists, p. 749–763.

Zonge, K.L., and Hughes, L.J., 1988, Controlled source audio-frequency magnetotellurics, *in* Nabighian, M.N., ed., Electromagnetic methods in applied geophysics: Society of Exploration Geophysicists, v. 2, p. 713–809.

Appendix 1

The figures in this appendix present the measured, calculated, and inverted data for each direct-current resistivity line. All data are displayed in units of resistivity. Figure 2 of this report shows the locations of the direct-current resistivity lines.

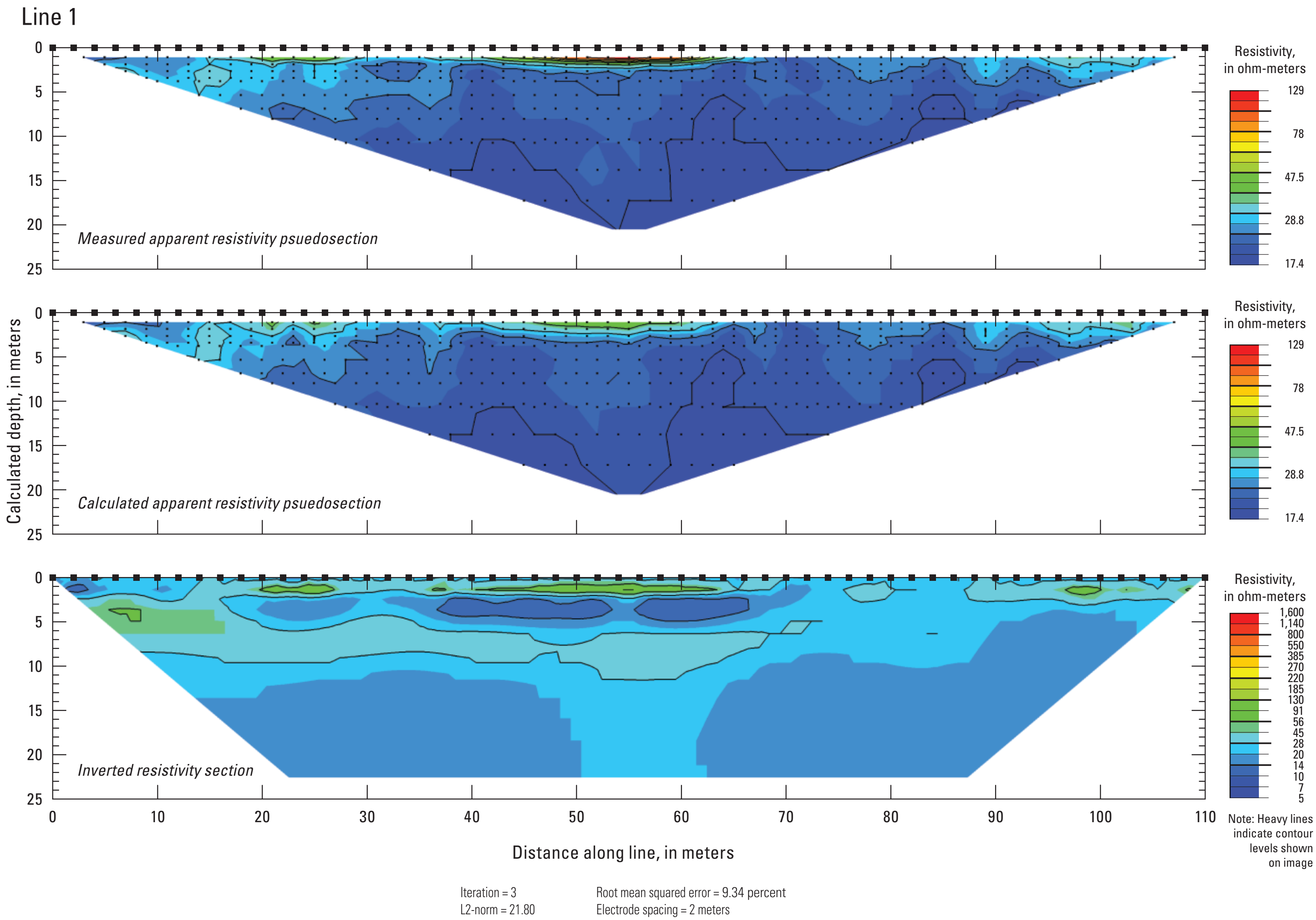

Figure 1–1. Measured, calculated, and inverted direct-current resistivity data collected along line 1 near the San Joaquin River, Merced County, California, 2012.

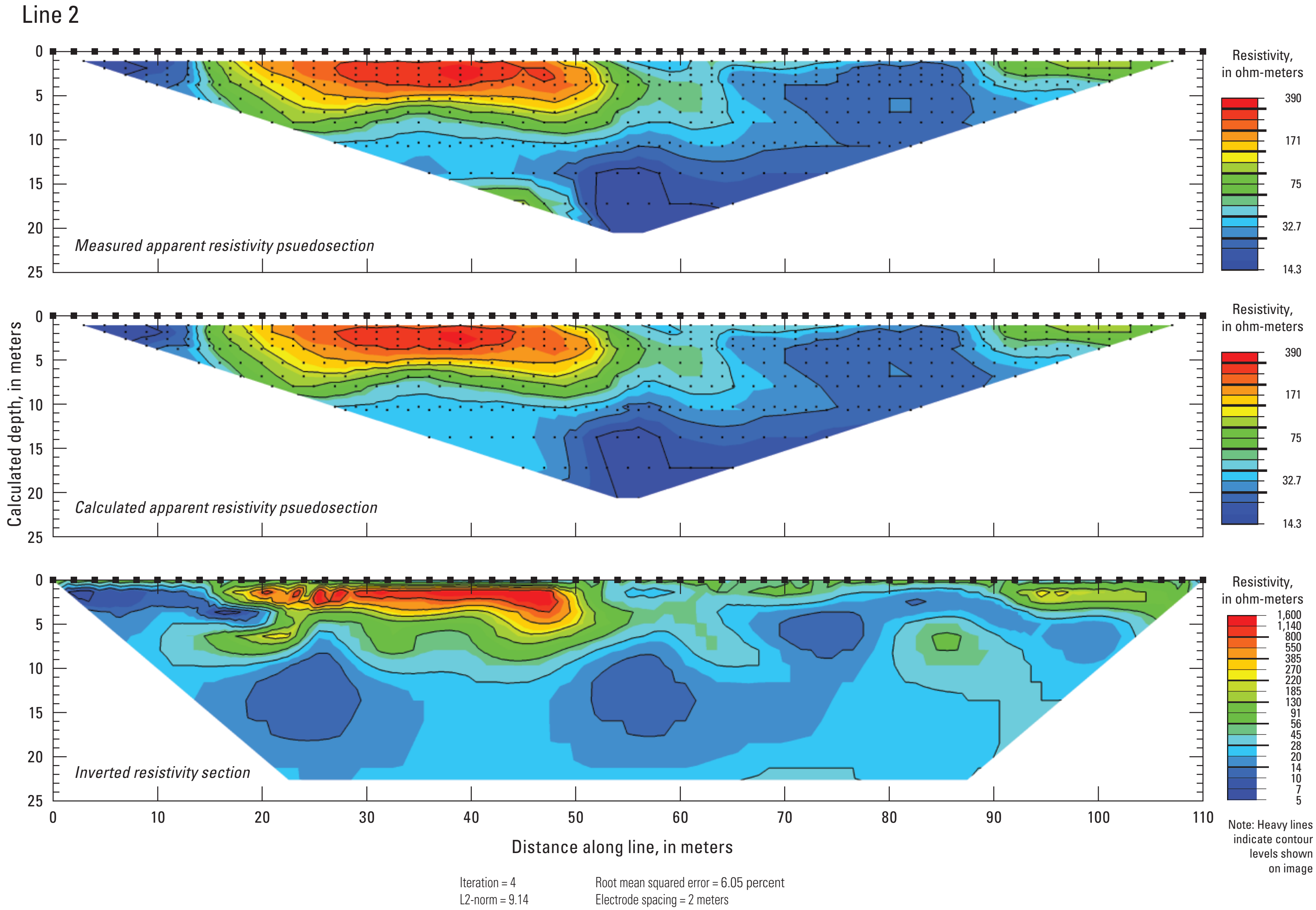

Figure 1–2. Measured, calculated, and inverted direct-current resistivity data collected along line 2 near the San Joaquin River, Merced County, California, 2012.

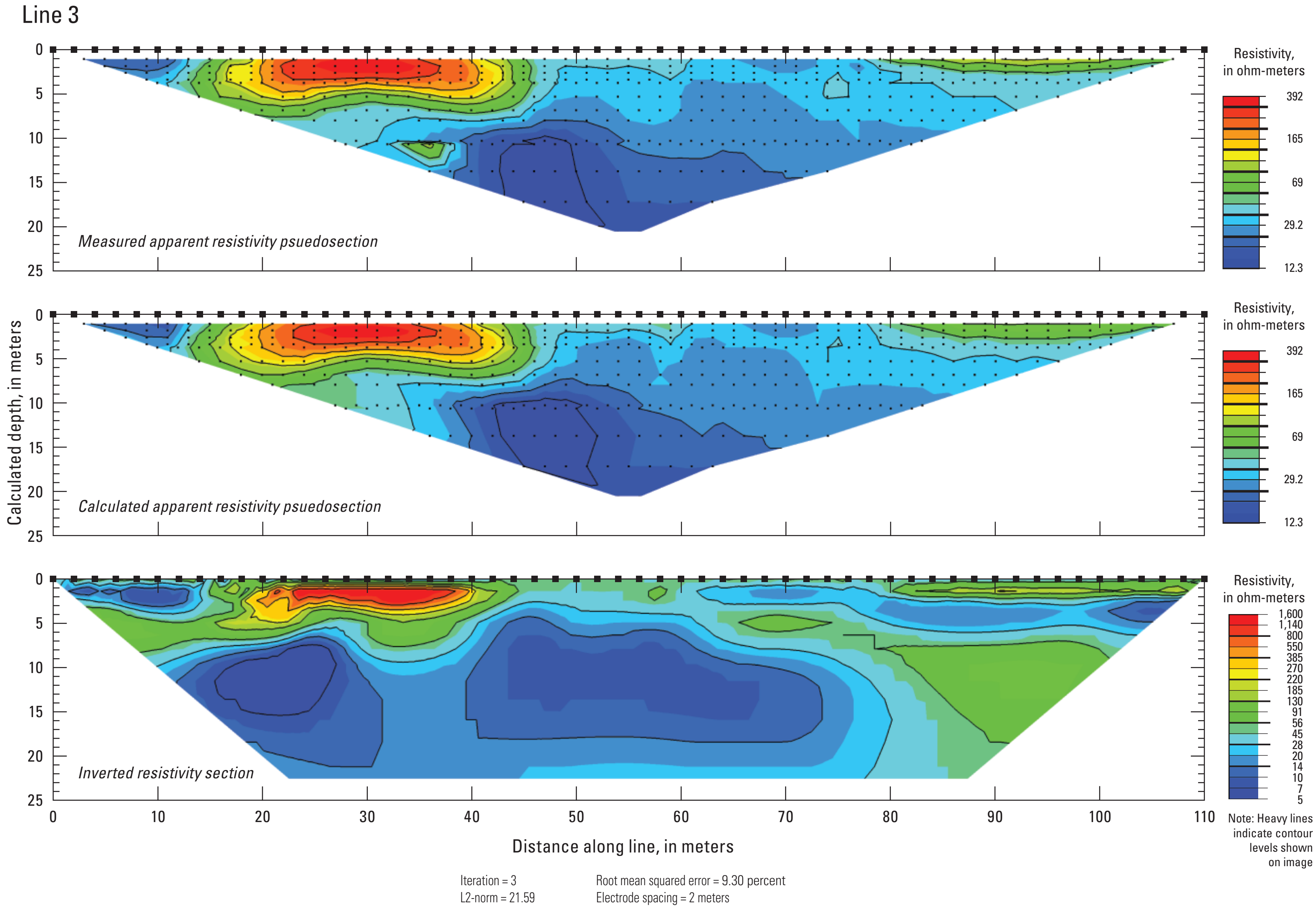

Figure 1–3. Measured, calculated, and inverted direct-current resistivity data collected along line 3 near the San Joaquin River, Merced County, California, 2012.

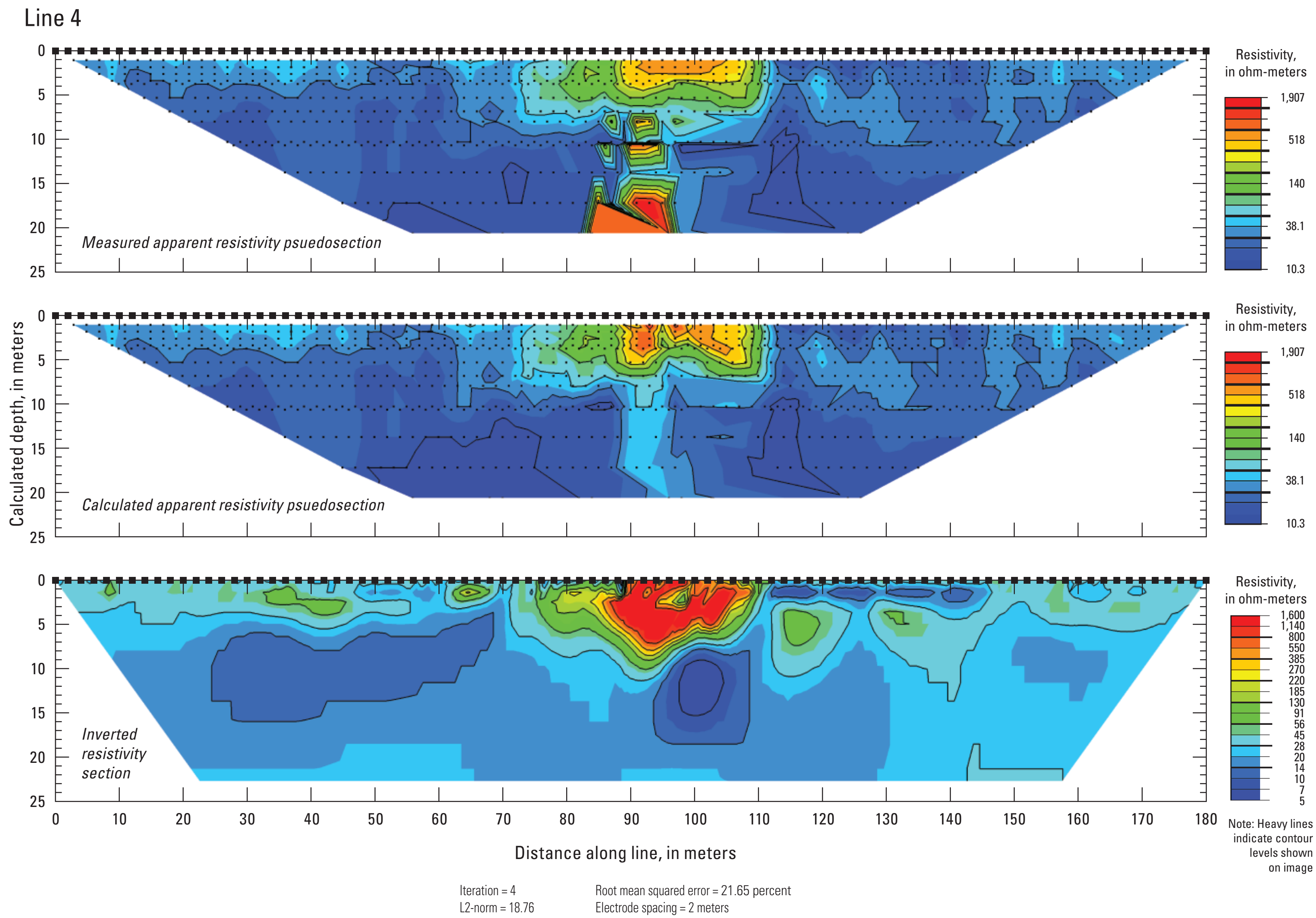

Figure 1–4. Measured, calculated, and inverted direct-current resistivity data collected along line 4 near the San Joaquin River, Merced County, California, 2012.

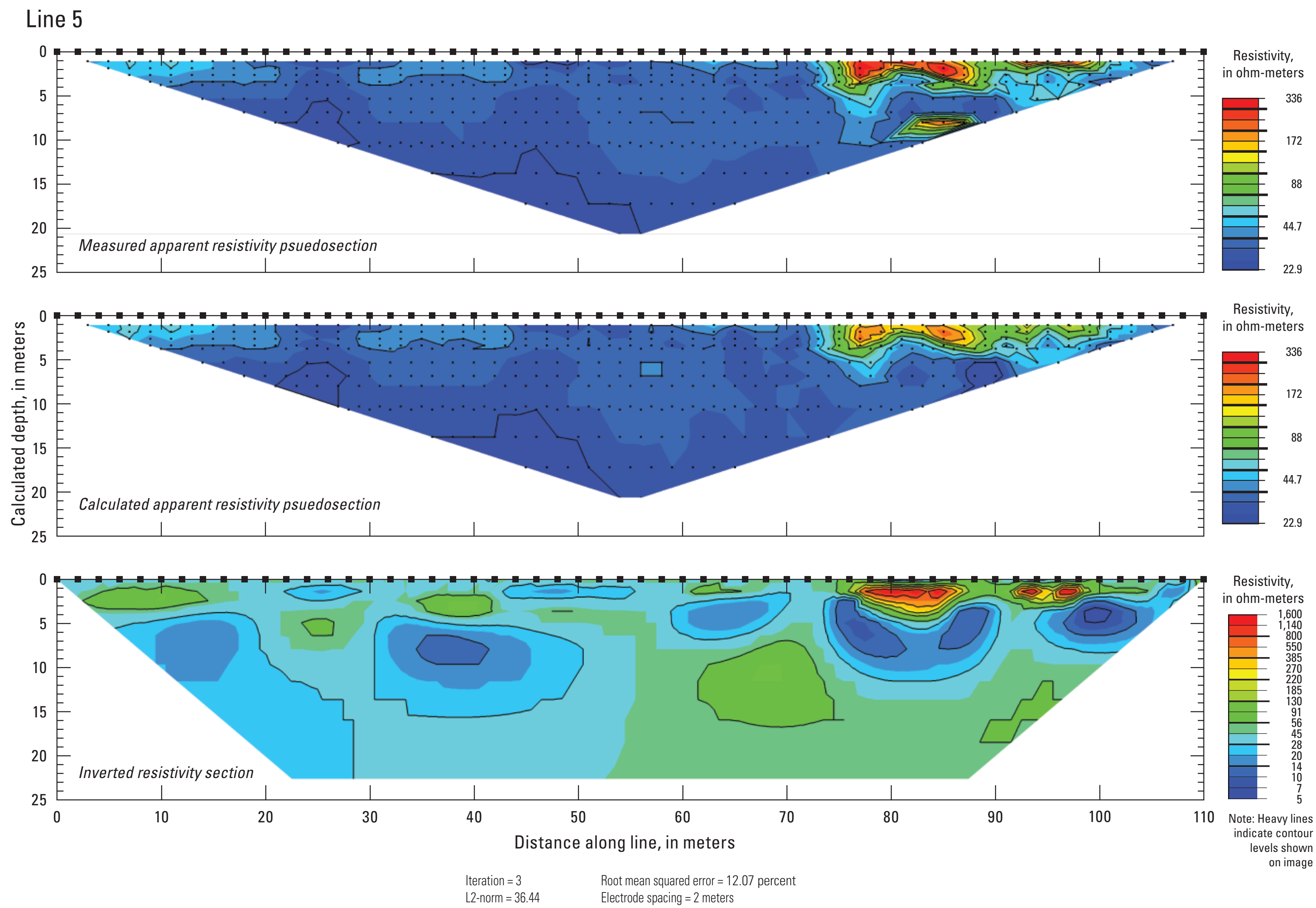

Figure 1–5. Measured, calculated, and inverted direct-current resistivity data collected along line 5 in the (dry) San Joaquin River, Merced County, California, 2013.

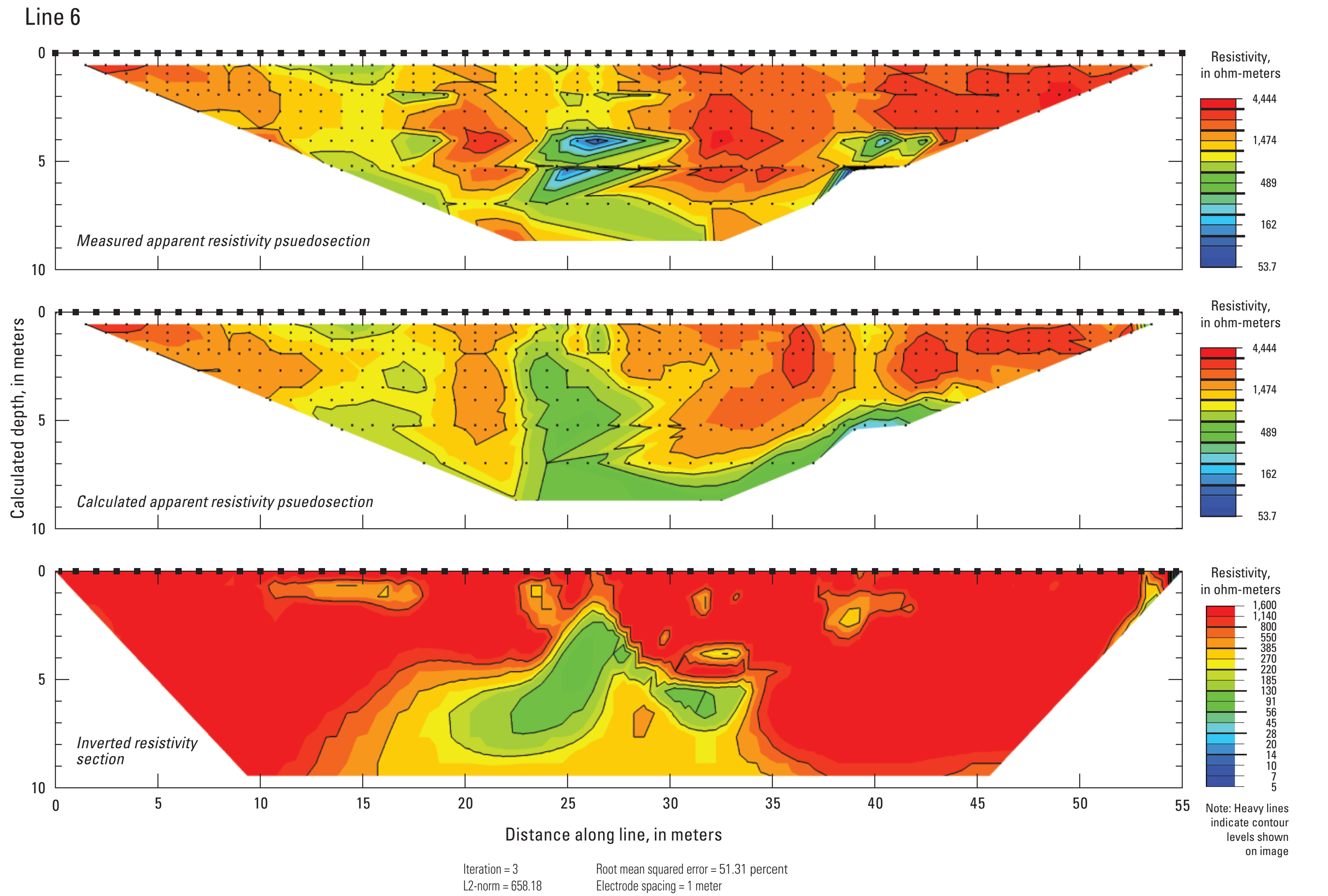

Figure 1–6. Measured, calculated , and inverted direct-current resistivity data collected along line 6 on the west bank of the San Joaquin River, Merced County, California, 2013.

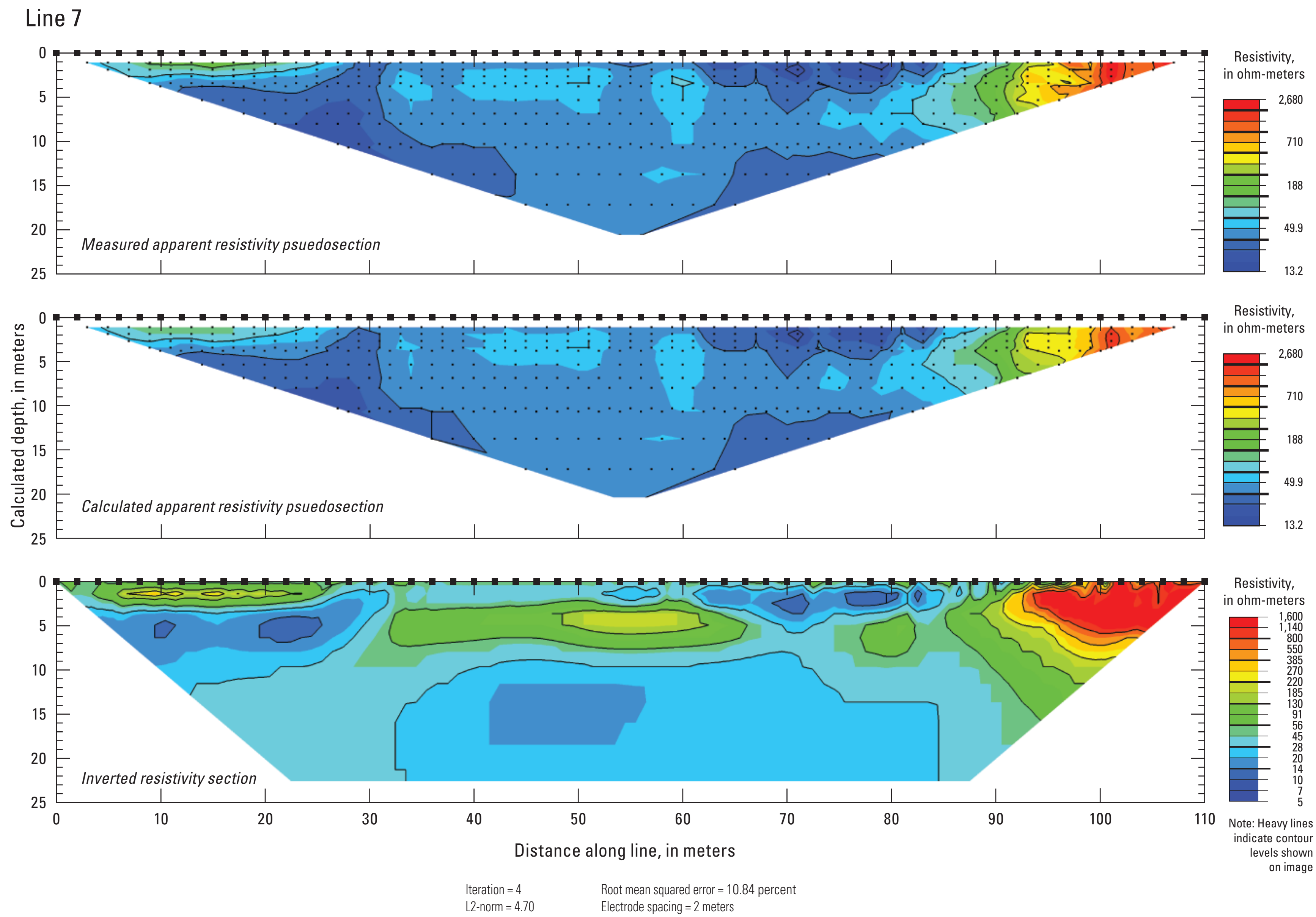

Figure 1–7. Measured, calculated, and inverted direct-current resistivity data collected along line 7 near the San Joaquin River, Merced County, California, 2013.

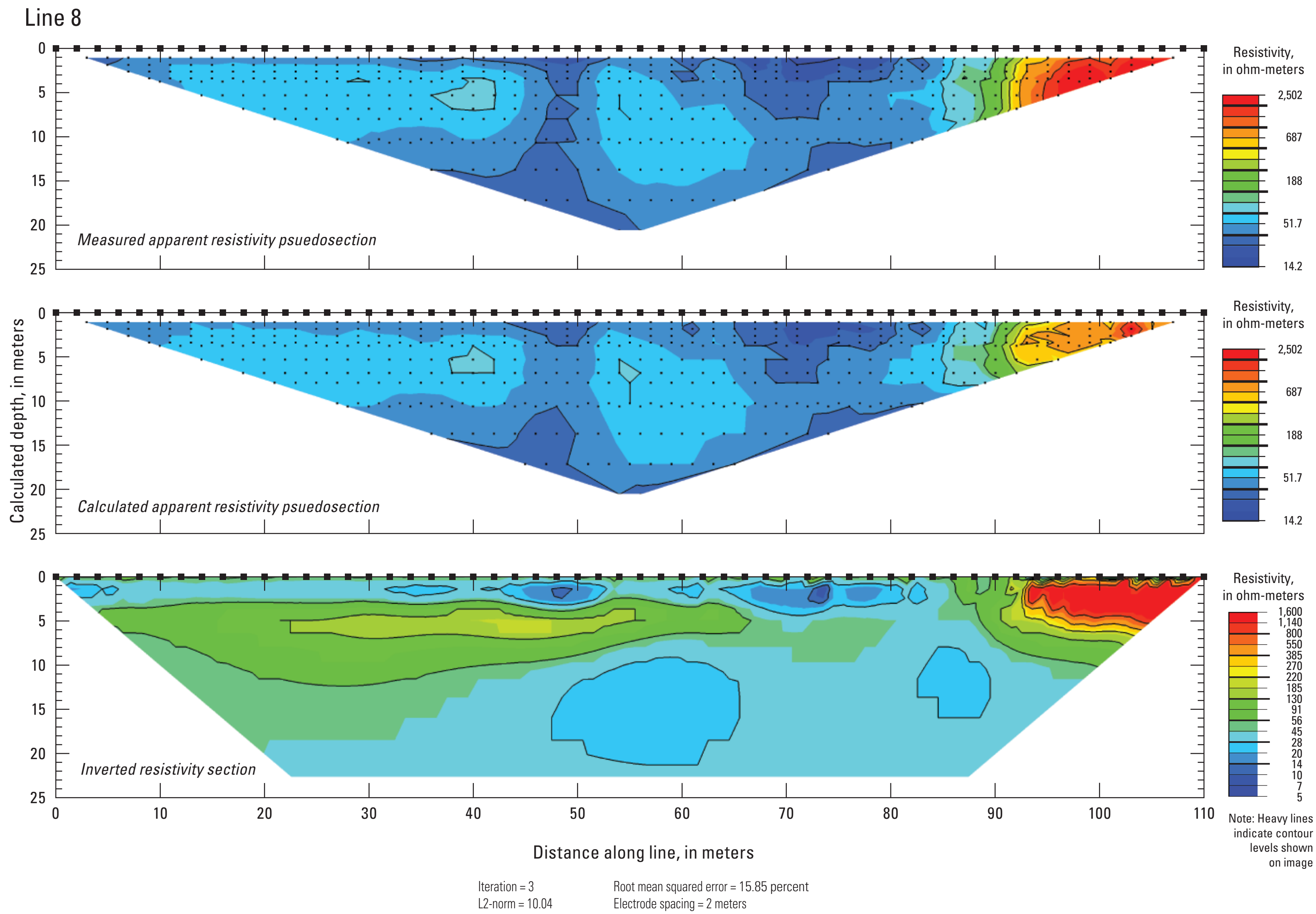

Figure 1–8. Measured, calculated, and inverted direct-current resistivity data collected along line 8 near the San Joaquin River, Merced County, California, 2013.

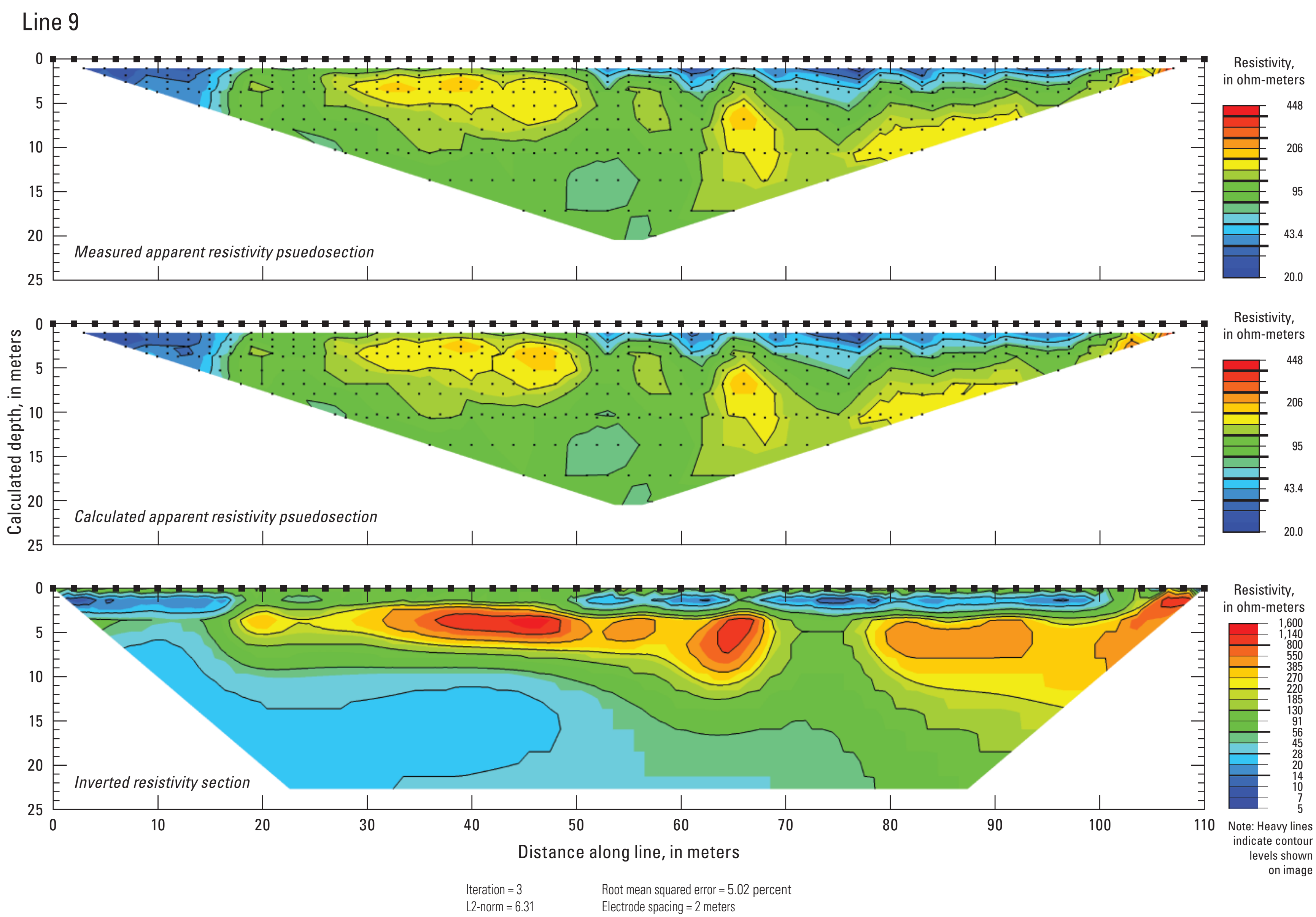

Figure 1–9. Measured, calculated, and inverted direct-current resistivity data collected along line 9 near the San Joaquin River, Merced County, California, 2013.

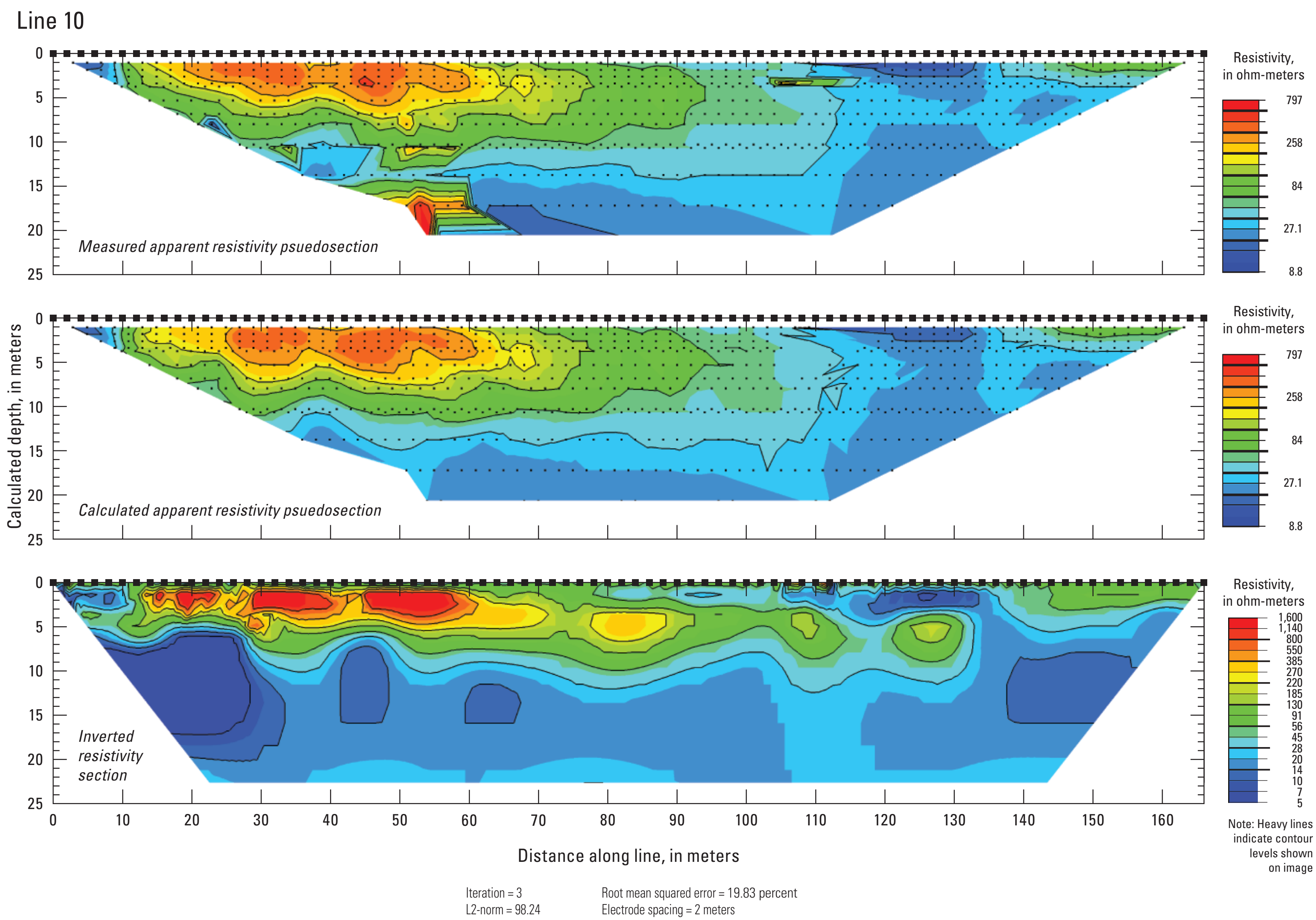

Figure 1–10. Measured, calculated, and inverted direct-current resistivity data collected along line 10 near the San Joaquin River, Merced County, California, 2013.

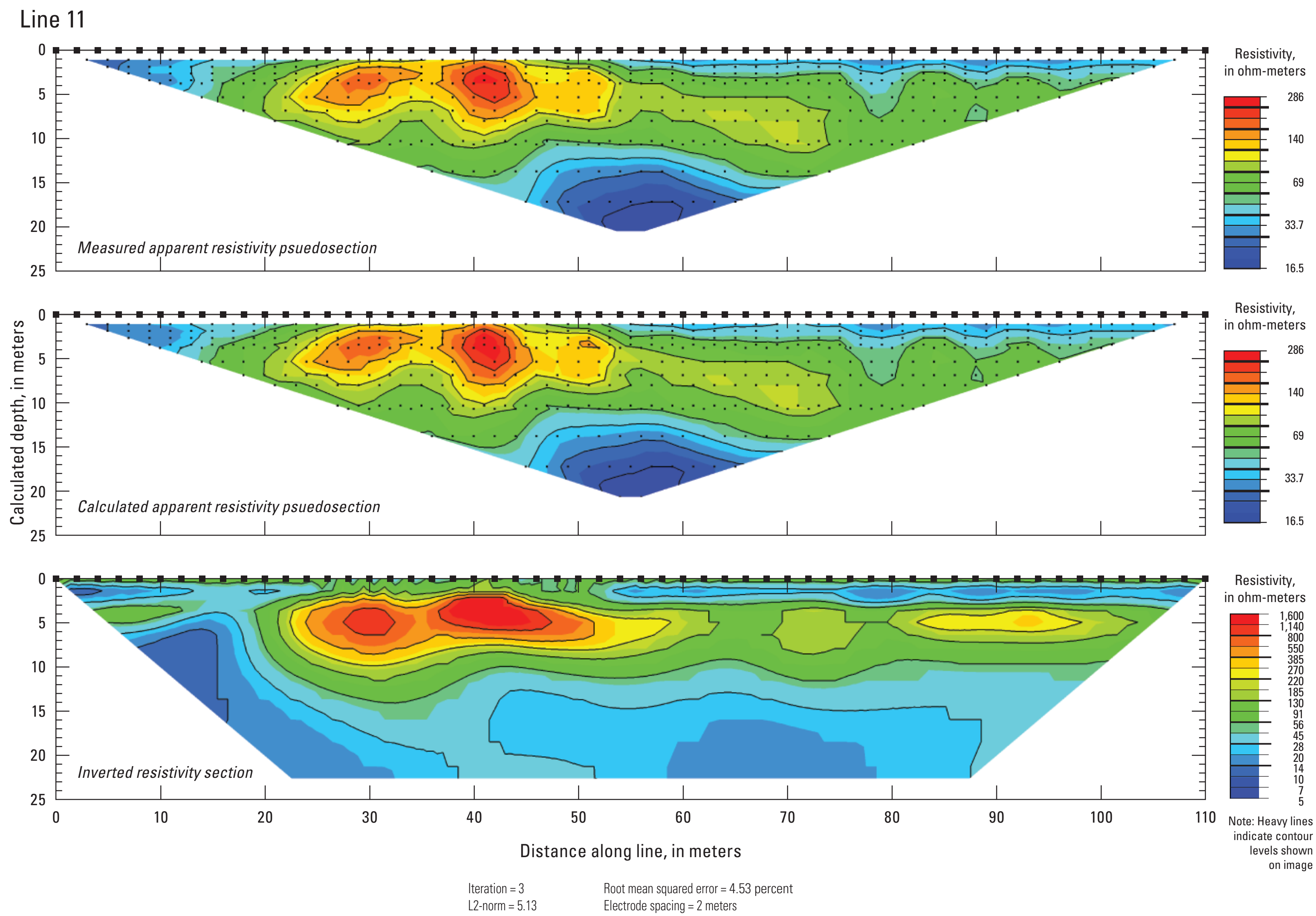

Figure 1–11. Measured, calculated, and inverted direct-current resistivity data collected along line 11 near the San Joaquin River, Merced County, California, 2013.

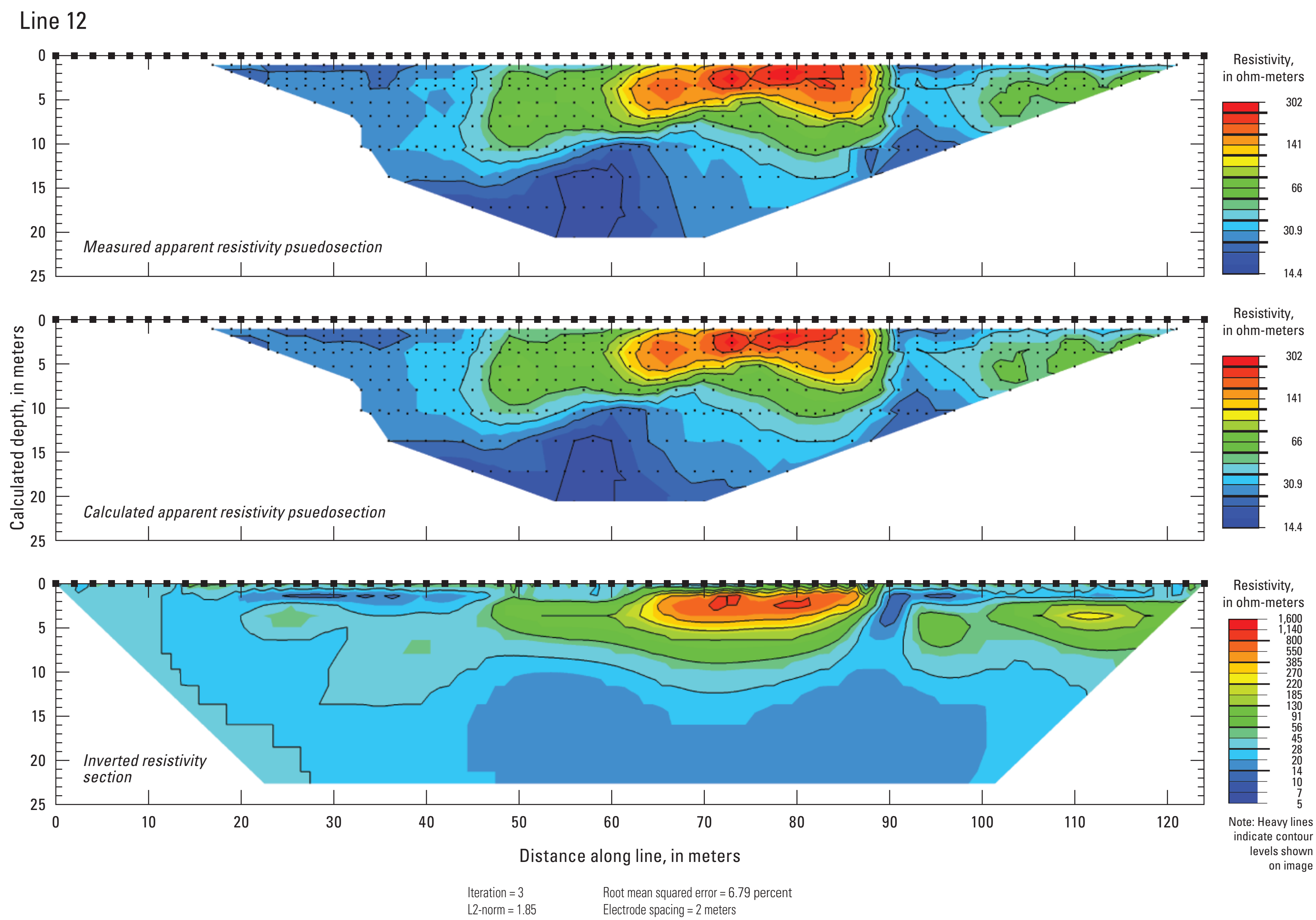

Figure 1–12. Measured, calculated , and inverted direct-current resistivity data collected along line 12 near the San Joaquin River, Merced County, California, 2013.

Publishing support provided by the U.S. Geological Survey
Science Publishing Network, Sacramento Publishing Service Center

For more information concerning the research in this report, contact the
Director, California Water Science Center
U.S. Geological Survey
6000 J Street, Placer Hall
Sacramento, California 95819
http://ca.water.usgs.gov

Groover and others—**Electrical Resistivity Investigation of Fluvial Geomorphology to Evaluate Potential Seepage Conduits to Agricultural Lands along the San Joaquin River, Merced County, California, 2012–13**—SIR 2016–5172

ISSN 2328-0328 (online)
https://doi.org/10.3133/sir20165172